Energy efficiency of membrane distillation up to high salinity: Evaluating critical system size and optimal membrane thickness

Citation: Swaminathan, Jaichander et al. "Energy Efficiency of Membrane Distillation up to High Salinity: Evaluating Critical System Size and Optimal Membrane Thickness." Applied Energy 211 (February 2018): 715–734 © 2017 Elsevier Ltd

As Published: http://dx.doi.org/10.1016/j.apenergy.2017.11.043

Publisher: Elsevier

Persistent URL: http://hdl.handle.net/1721.1/113008

Version: Author's final manuscript: final author's manuscript post peer review, without publisher's formatting or copy editing

Energy efficiency of membrane distillation up to high salinity: evaluating critical system size and optimal membrane thickness *

Jaichander Swaminathan, Hyung Won Chung, David M. Warsinger, John H. Lienhard V*

Rohsenow Kendall Heat Transfer Laboratory, Department of Mechanical Engineering, Massachusetts Institute of Technology, Cambridge MA 02139-4307 USA

Abstract

This study presents a comprehensive analytical framework to design efficient single-stage membrane distillation (MD) systems for the desalination of feed streams up to high salinity. MD performance is quantified in terms of energy efficiency (represented as a gained output ratio, or GOR) and vapor flux, both of which together affect the specific cost of pure water production. Irrespective of the feed salinity, permeate or conductive gap MD (P/CGMD) performs better than direct contact MD (DCMD) when the heat transfer resistance of the gap (in P/CGMD) is lower than that of the external heat exchanger in DCMD. Air gap MD's (AGMD) better performance relative to the other configurations at high salinity and large system area can be explained in terms of its thicker 'effective membrane', which includes the air-gap region. CGMD and DCMD employing a thick membrane are also resilient to high salinity, similar to AGMD, while not being susceptible to the gap flooding that can harm AGMD's performance. A method is described to simultaneously determine the cost-optimal membrane thickness and system size as a function of the ratio of specific costs of heat energy and module area. At low salinity and small system size, GOR rises and flux declines with an increase in membrane area. For salty feed solutions, there exists a critical system size beyond which GOR also begins to decline. Since both GOR and flux are lower, no economic rationale favors operation above this critical size, irrespective of the costs of thermal energy and system area. A closed-form analytical expression for this critical system area is derived as a function of the feed salinity and two dimensionless ratios of heat transfer resistances within the MD module.

Keywords: membrane distillation, high salinity, energy efficiency, system size, optimal membrane thickness

*Corresponding author: lienhard@mit.edu

*Citation: J. Swaminathan, H.W. Chung, D.M. Warsinger, J.H. Lienhard V, "Energy efficiency of membrane distillation at high salinity: evaluating critical system size and optimal membrane thickness," Applied Energy, online 24 Nov. 2017, 211:715734, 1 Feb. 2018.

I. Unified modeling of MD configurations

Equivalent parameters:

Direct Contact	**Flooded Air Gap** or **Conductive Gap**	**Air Gap**
external HX thermal reistance $1/U_{\mathrm{HX}}A_{\mathrm{HX}}$	gap thermal resistance $d_{\mathrm{gap}}/k_{\mathrm{gap}}A_{\mathrm{m}}$	condensate film thermal resistance $d_{\mathrm{film}}/k_{\mathrm{film}}A_{\mathrm{m}}$
membrane thickness δ_{m}		thickness of (membrane + air gap) $\delta_{\mathrm{m}} + d_{\text{air-gap}}$

II. Dimensionless design framework

Derived GOR = f(dimensionless parameters)

Identified critical system size, to avoid low flux and low energy efficiency

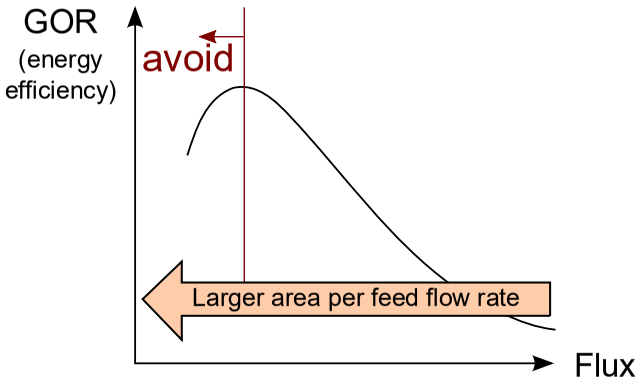

Nomenclature

Acronyms

AGMD	Air gap membrane distillation
CGMD	Conductive gap membrane distillation
DCMD	Direct contact membrane distillation
GOR	Gained Output Ratio
HX	Heat Exchanger
LMH	L/m^2·hr
MD	Membrane distillation
NTU	Number of transfer units
PGMD	Permeate gap membrane distillation
P/CGMD	Permeate or conductive gap membrane distillation
TTD	Terminal temperature difference, °C

Roman Symbols

A	Area, m^2
a_{w}	Activity of water
B	Membrane permeability, kg/m^2·s·Pa
B_0	Membrane permeability coefficient, kg/m·s·Pa
c	Specific cost, \$/m^3, \$/kWh or \$/m^2
C	Cost factor
c_p	Specific heat capacity, J/kg·K
d	Depth or thickness, m
ΔT_{VPD}	Measure of vapor pressure depression due to dissolved salts, °C
ΔT_{BPE}	Boiling point elevation, °C
h	Heat transfer coefficient, W/m^2·K
h_{fg}	Enthalpy of vaporization, J/kg
J	Permeate flux, L/m^2·hr
k	Thermal conductivity, W/m·K
L	Length of module, m
m	Molality, mol/kg-solvent
$\dot{m}$	Mass flow rate, kg/s
$\dot{Q}$	Heat transfer rate, W
$\dot{q}$	Heat flux, W/m^2
p^{vap}	Vapor Pressure, Pa
R	Thermal resistance, K/W

s	Salinity, g/kg
T	Temperature, °C
U	Overall heat transfer coefficient, W/m^2·K
v	Velocity, m/s
w	Width, m
Y	Non-dimensional resistance ratio

Greek Symbols

δ_{m}	Membrane thickness, m
ε	Exchanger effectiveness
η	Thermal efficiency
ϕ	Porosity
$\phi_{\mathrm{ch:m}}$	Non-dimensional resistance ratio
$\phi_{\mathrm{c:v}}$	Non-dimensional resistance ratio

Subscripts, Superscripts

b	Bulk stream
c	Cold channel
ch	Channel - feed, cold or gap
cond	Conduction
crit	Critical size
eff,m	effective property of membrane
f	Feed channel
gap	Gap between membrane and condensing surface
HX	Heat exchanger
in	Inlet
m	Membrane
max	Maximum
MD	Membrane distillation module
min	Minimum
out	Outlet
p	Permeate
ph	Preheating stream
sat	Saturated state
vap	Vapor
VPD	Vapor Pressure Depression
w	Wall

1. Introduction

Membrane distillation (MD) is a thermal desalination technology that is especially promising for high-salinity streams of $s_f \approx 70$–300 g-salt/kg-solution, where conventional reverse osmosis is not currently applied. This study develops a unified analytical description of single-stage MD configurations based on the heat transfer resistances in various portions of the MD module. The configurations evaluated are direct contact, permeate or conductive gap, and air gap MD. Using this framework, two important aspects of designing efficient MD systems for desalination up to high salinity are analyzed:

1. the choice of the best MD configuration for a given desalination application; and
2. system design and operation that avoids conditions of low flux and low energy efficiency.

As a related exercise, a method to identify the cost-optimal membrane thickness is developed. The novelty of this work lies in developing a unified description of several single-stage MD configurations by replacing a large number of design and operation variables with a few dimensionless parameters, and deriving an expression for maximum allowable system area as a function of these parameters.

1.1. Context: desalination up to high salinity

Seawater, brackish groundwater, and municipal wastewater streams are commonly desalinated to produce potable grade water. In these cases, the maximum salinity of the brine is often restricted, by the available technology, to be less than 70 g/kg. In other applications (e.g., industrial zero-liquid-discharge, inland brine management, and concentration of produced water from hydraulic fracturing), brines with salinities between 50 g/kg and saturation concentration may have to be further desalinated. Conventional spiral wound reverse osmosis (RO), the workhorse of the desalination industry today, is typically operated below 70 bar of applied pressure [1]. As a result, RO is not directly applicable to desalination of these saltier streams for which the osmotic pressure can be as high as 300 bar [2].

Thermal separation processes such as mechanical vapor compression (MVC) are often used for such applications [3, 4], since desalination up to saturation concentration is possible in these systems at low pressures and temperatures ($< 100\,^{\circ}\mathrm{C}$). More recently, humidification dehumidification desalination (HDH) [5, 6, 7, 8] has been developed as simple, low capital-cost thermal technology for treating ultra-saline produced waters [9, 10].

Membrane distillation (MD) is a thermally driven, scalable desalination process [11, 12] that has been identified as a candidate technology for modular desalination of high-salinity brines [13, 14, 15]. Since MD can operate at low feed temperatures, it has been successfully coupled with a range of renewable energy sources [16, 17, 18, 19]. MD has been experimentally and numerically investigated for high-salinity applications, mostly using small-scale systems. A unified perspective on MD system design for high salinity is lacking and is therefore the focus of this study.

In the reminder of this section, some key MD performance metrics are discussed while reviewing previous studies of MD up to high salinity.

1.2. Membrane distillation studies at high salinity

1.2.1. Small area systems measuring flux and thermal efficiency

Most studies have focused on small membrane area systems because of their ease of fabrication at a lab-scale. The negative impact of high salinity on water flux in small systems has been widely reported [20, 21, 22]. Guan et al. [23], Li et al. [24], and Alkhudhiri et al. [25] tested MD with various electrolyte solutions up to high salinity and found that water activity is a good predictor of the pure water flux. Vapor pressure at the solution-vapor interface is proportional to the activity of water, which declines with increasing feed salinity and does so at a different rate for each electrolyte solution.

In addition to water flux, the effect of high salinity on MD thermal efficiency (η) has also been investigated through experimental [26, 27] and numerical [28] techniques. The thermal efficiency is the fractional contribution of vapor transport to the overall energy transfer across the membrane [29]:

$$\eta = \frac{\dot{Q}_{\mathrm{vap}}}{\dot{Q}_{\mathrm{vap}} + \dot{Q}_{\mathrm{cond}}} \tag{1}$$

where $\dot{Q}_{\mathrm{vap}}$ is the energy transfer by vapor and $\dot{Q}_{\mathrm{cond}}$ is the heat conducted through the membrane. A low value of η indicates significant heat conduction loss through the membrane and values approaching 1 are desirable.

An interesting application of high salinity MD is the MD crystallizer system in which pure water is extracted from a supersaturated solution using MD with the brine recirculated into a tank where salt is precipitated [30, 31].

1.2.2. Large area systems measuring GOR and flux

With the availability of commercial, larger size MD modules, studies of energy efficiency (which can be represented as a gained output ratio, GOR) have also become more numerous. GOR is a non-dimensional measure of the water production per unit of thermal energy consumption [32]:

$$\mathrm{GOR} = \frac{\dot{m}_{\mathrm{p}} h_{\mathrm{fg}}}{\dot{Q}_{\mathrm{h}}} = \eta \, \frac{\varepsilon}{1-\varepsilon} \tag{2}$$

While GOR is proportional to MD thermal efficiency η, it is also strongly affected by the extent of feed preheating, and this effect is captured by the exchanger effectiveness: $\varepsilon = (T_{\mathrm{ph,out}} - T_{\mathrm{ph,in}})/(T_{\mathrm{f,in}} - T_{\mathrm{ph,in}})$ (temperatures shown in Fig. 1). For gap MD systems, feed preheating happens within the module where the feed acts as a coolant in contact with the condensation surface. In direct contact MD (DCMD), preheating takes place in an external heat exchanger (HX), where the warm pure water stream leaving the module heats the incoming feed.

While η quantifies the efficiency of energy transfer across the membrane, GOR is a global measure of the system's energy efficiency because a higher GOR directly corresponds to lower energy use per unit of distillate produced. Therefore, GOR is a more comprehensive measure of energy efficiency, and along with flux, will be used to quantify system performance. In vacuum MD, conduction across the membrane is typically neglected

because of the vacuum [29], resulting in $\eta = 1$. Chung et al. [33] modeled a multistage vacuum membrane distillation process up to high salinity and found that GOR and water productivity significantly decrease with salinity even though η is constant.

Recently, Deshmukh and Elimelech [34] numerically studied the DCMD process at high salinity and highlighted that membrane improvement should focus on increasing the membrane's ratio of vapor permeability to thermal conductivity, similar to earlier findings by Martínez and Rodríguez-Martoto [35]. They also analyzed the relative impact of modifying various membrane physical properties in this regard.

Winter et al. [36] measured flux and specific thermal energy consumption for spiral-wound PGMD modules up to 105 g/kg. At higher salinity levels, a peak value of GOR was observed with changing in feed inlet flow rate. Similarly, Thiel et al. [2] used numerical models of PGMD to illustrate the existence of an optimal system size (represented through a terminal temperature difference) at which GOR is maximized when the feed inlet flow rate is held constant.

The studies mentioned in the previous paragraphs identify the existence of a critical feed flow rate (for a system of fixed size) or equivalently a critical system size (for a fixed inlet feed flow rate), at which GOR is maximized. Reducing the feed flow rate or increasing system size beyond this critical value leads to a decrease in both GOR and flux. Such an operating condition is unfavorable irrespective of the costs of thermal energy and system area. In Section 3.3, an expression for this critical system size relative to the feed inlet flow rate is derived to help avoid such unfavorable operation.

1.3. Choice of MD configuration

Figure 1 is a schematic representation of various single stage MD systems. In AGMD, there exists an air gap between the membrane and condensation surface. This gap is filled completely with distillate in PGMD. In CGMD, the gap is made thinner and a high thermal conductivity material is used to enhance its overall conductance across the thickness direction. In all these gap MD systems, the feed stream is preheated as it flows across the condensation surface. In DCMD, the vapor from the feed side condenses into a cooler pure water stream flowing on the other side of the membrane. Warm pure water leaving the MD module preheats the feed in a separate external HX.

The relative performance of the MD configurations needs to be understood in order to choose the appropriate configuration for a given application. Several authors have contrasted the performance of AGMD and DCMD in small-scale systems, highlighting AGMD's higher η and DCMD's higher flux [37]. Recently, Eykens et al. [38] experimentally demonstrated that the sensitivity of flux to various process conditions (such as temperature, feed velocity, and salinity) is configuration dependent.

Winter [39] reported results from pilot-scale modules for AGMD, PGMD, and DCMD. He found that the GOR and flux of PGMD and DCMD were close, and higher than that of AGMD. AGMD performance was more resilient to an increase in feed salinity, whereas the performances of DCMD and PGMD dropped faster. No clear hierarchy was established between PGMD and DCMD.

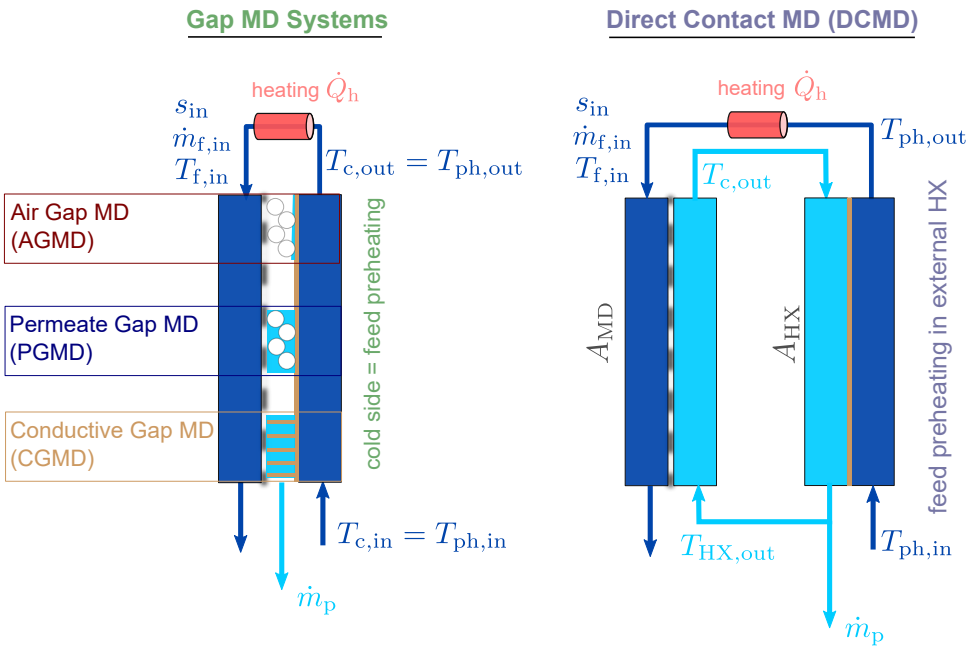

Figure 1: A schematic representation of the single stage MD configurations considered in this study. AGMD, PGMD and CGMD differ based on the gap conditions. DCMD requires an external HX for feed preheating (which is indicated by the subscript 'ph').

1.3.1. Comparison methodology in this study

Swaminathan et al. [32] used performance curves in the energy efficiency-flux plane to compare 'balanced' counterflow [40, 41] single-stage MD configurations. For seawater salinity and the baseline parameters considered, they showed that CGMD performance corresponds to the practical upper limit of PGMD (with a low gap thickness) and DCMD (with a large external HX). Additionally, AGMD's performance was close to that of PGMD.

The rationale behind plotting the performance of systems in a GOR-flux plane is that the cost of pure water production or brine concentration is always affected by both capital expenses (CapEx) and operating expenses (OpEx). The specific cost of pure water production ($c_{sp,water}$) using MD can be expressed as a function of GOR and flux as (see Appendix A.1):

$$c_{sp,water} = \frac{C_{GOR}}{GOR} + \frac{C_{flux}}{J} \tag{3}$$

where C_{GOR} is the scaled specific cost of thermal energy, C_{flux} is the scaled and amortized specific cost of system area, and J is the pure water flux in L/m^2·hr (or LMH). In this equation, the first term corresponds to the operating expenditure (cost of heat), and the second term corresponds to capital expenditure. Some studies of the economics of MD neglect the cost of thermal energy assuming that a free source of low-grade "waste" heat may be available [42]. Many membrane tests at small scale have also focused exclusively on water flux. In reality, the cost of providing thermal energy is usually quite significant [43]. Even if a waste-heat source is available, the cost of equipment such as heat exchangers required to access the waste heat

must be accounted for and will contribute to a non-zero value of C_{GOR}.

With increasing system size, GOR usually increases and flux decreases. When performances are plotted on GOR-flux axes, GOR and flux can be simultaneously compared while allowing system size to vary. This comparison of GOR at the same flux level is based on Eq. 3 and assumes that C_{GOR} and C_{flux} are similar across different configurations. C_{GOR} is only influenced by the source of thermal energy and is truly independent of MD configuration. Some variability in C_{flux} can be associated with the design choices. Compared to the baseline case of AGMD:

- In PGMD, the gap is filled with liquid water - this should not result in a difference in C_{flux}.
- In CGMD, the thermal conductance across the thickness of the water-filled gap is enhanced. This can be achieved by introducing fins on the condensation surface or designing a thermally conductive spacer, and making the gap thinner. The additional metal used to improve gap conductance can increase C_{flux}, but this increase is likely to be small since the gap is quite thin.
- In DCMD, the amount of metal in the external HX can be different from that in the condensation surface of AGMD. An additional pump is required for the cold loop, whereas there is only one flow loop in the other MD configurations. The total pumping power is also likely to be higher in DCMD due to additional flow resistance in the HX flow channels and fittings.

  In a previous study [32], in order to perform a fair comparison, the heat transfer area in the external HX was assumed to be equal to that of the condenser surface area ($= A_{\mathrm{m}}$), and the effect of $A_{\mathrm{HX}}/A_{\mathrm{m}}$ was evaluated separately.

A given desalination application can be described in terms of the feed water properties (e.g., s_{f}), ambient temperature ($T_{\mathrm{ph,in}}$), heater output temperature ($T_{\mathrm{f,in}}$), and costs of MD module and thermal energy (C_{flux}, C_{GOR}). The membrane, feed channel geometry, and feed inlet velocity (and correspondingly, heat transfer coefficients $h_{\mathrm{f}}, h_{\mathrm{c}}$) are assumed constant across the different systems to enable a fair comparison.

1.3.2. Choice of membrane thickness

Pure water flux is driven by a difference in vapor pressure between the evaporation and condensation liquid-vapor interfaces and is proportional to the membrane permeability, B. The difference in vapor pressure is influenced by the temperature difference between these two interfaces, ΔT_{m}, and feed salinity, $s_{\mathrm{f,m}}$. Heat conduction loss across the membrane is only a function of ΔT_{m}. Membrane permeability is inversely proportional to membrane thickness, δ_{m}. As thickness is decreased, vapor flux when desalinating salty water initially increases (due to higher permeability), but starts declining as a result of conduction losses when thickness goes below an optimal value. Below this optimal thickness, ΔT_{m} across the module becomes comparable to the feed boiling point elevation, ΔT_{BPE}. As a result, mass transfer is inhibited and heat conduction losses become dominant. For distillation of very low salinity water, the membrane ought to be as thin as possible. However, the optimal membrane thickness is larger for higher salinity feed water [44].

Several authors have considered the question of optimal membrane thickness, especially in the context of maximizing flux in DCMD. For a small area DCMD module, at fixed hot and cold side temperatures and feed salinity, an ideal value of membrane thickness can be determined to maximize flux [27, 45].

Ali et al. [46] evaluated the optimal membrane thickness for multiple values of system size at a fixed salinity. They show that, for smaller system size, a thin membrane maximizes flux, whereas as the system size increases, the driving temperature difference (ΔT_{m}) decreases, thereby making the optimal membrane thickness larger.

Winter [39] evaluated the optimal thickness for large scale spiral wound modules under two operating conditions: high recovery and high flux. A numerical model was used to infer optimal membrane thicknesses for a given system size and feed inlet flow rate over a range of salinity levels. Two kinds of optima were identified - one that maximizes GOR and another that maximizes flux.

Identifying an optimal membrane thickness is an inherent part of MD system design. It should therefore be considered together with the choice of optimal system size, rather than independently. In Section 2.4, the effect of δ_{m} on the GOR-flux performance curve is used to identify an optimal membrane thickness as a function of $C_{\mathrm{GOR}}/C_{\mathrm{flux}}$.

1.4. Manuscript overview

In part 1 (Section 2), the equivalence of various single-stage MD configurations in terms of overall performance is established by considering the heat transfer resistances in different portions of the module. First, in Section 2.2, a clear performance hierarchy is established among DCMD and P/CGMD based on the thermal resistance of the external HX and of the gap. Thereafter, in Section 2.3, the difference in AGMD performance relative to the other configurations is explained by identifying that the air gap results in an effectively thicker membrane. A method to determine optimal membrane thickness along with optimal system size is described in Section 2.4.

In part 2, a simplified HX analogy model of single-stage MD is used to understand the dimensionless groups affecting performance. An expression is derived for the critical specific area of an MD system, $\mathrm{NTU}^{\mathrm{crit}}$, above which both energy efficiency and flux are poor (Section 3.3). Low GOR and flux can be avoided by choosing membrane area appropriately at the design stage or by adjusting the flow rate during operation.

2. Part 1: Unified framework for single stage MD configurations

2.1. Methodology: discretized numerical model

A length-wise discretized finite difference modeling framework (referred to here as a 1-D model) is used, which has been described and validated previously [32, 47, 48]. Model features that are particularly relevant to high salinity are discussed here. Pure sodium chloride solution up to 260 g/kg is considered as the feed. To account for the nonlinear effect of high feed salinity on vapor pressure, Pitzer's equations [49] describing the

properties of aqueous NaCl solution were used to evaluate water activity and thereby water vapor pressure on the feed side:

$$p_{\mathrm{vap}}^{\mathrm{f,m}} = P_{\mathrm{sat}}\left(T_{\mathrm{f,m}}\right) \times a_{\mathrm{w}}\left(s_{\mathrm{f,m}}, T_{\mathrm{f,m}}\right) \tag{4}$$

The specific heat capacity of water changes significantly with salinity and so this effect is also incorporated. The enthalpy of aqueous sodium chloride solution is obtained as a polynomial fit over $T \in [20, 90]\,^{\circ}\mathrm{C}$ and $s \in [0, 260]$ g/kg from the Pitzer model. Similarly, the effect of increased salinity on feed thermal conductivity is included.

Since the goal of this analysis is to provide system-level insights and compare various configurations, other effects of high salinity (e.g., on liquid viscosity) are not considered. The membrane is characterized by an average permeability coefficient (B_0), thickness (δ_{m}), porosity (ϕ), and membrane material conductivity (k_{m}). Permeability to vapor (B) can be expressed as B_0/δ_{m}. The baseline values of system properties are listed in Table A.2. The feed salinity is varied from 50–260 g/kg, which is the relevant range of salinities for brine-concentration applications.

The effect of feed salt concentration on AGMD flux was experimentally evaluated. The module design is detailed elsewhere [50] and is chosen to achieve constant temperature, salinity, and flowrate over the active membrane area. Figure 2a plots measured flux as a function of inlet feed salinity, showing that model predictions of flux in the small-area system are in good agreement with the experiment data. The following parameters were used in the model (consistent with previous fitting of model performance at low salinity): $T_{\mathrm{f,in}} = 70.4\,^{\circ}\mathrm{C}$, $T_{\mathrm{c,in}} = 19.5\,^{\circ}\mathrm{C}$, $\dot{Q}_{\mathrm{f}} = 15.1$ L/min, $\dot{Q}_{\mathrm{c}} = 13.9$ L/min, $B = 16 \times 10^{-7}$ kg/m^2·s·Pa, $d_{\mathrm{gap}} = 0.75$ mm, $k_{\mathrm{m}} = 0.2$ W/m·K, $\delta_{\mathrm{m}} = 200$ μm, $\phi_{\mathrm{m}} = 0.8$. The average and maximum deviation between the model predictions and experimental results are 5.1% and 11.4%. The deviation increases at high salinity which could be due the larger effect of heat loss at high salinity when the feed specific heat is lower, or higher inaccuracy in measurement of flow-rate or salinity.

Figure 2b shows comparisons of present model predictions to other reported data [39] for the effect of feed salinity on overall energy efficiency of larger, spiral wound MD modules. The model conditions are the same as those used in [32] for comparing the effect of feed inlet temperature and flow rate. The model captures the trends observed experimentally: GOR of PGMD and DCMD are close, start higher than AGMD at low salinity, but also decline faster with increasing salinity. In contrast, the AGMD module's GOR remains relatively constant over the entire salinity range. The average absolute deviation is 5.3% excluding one data point at low absolute magnitude of GOR for which the deviation is 45.2%.

2.2. Ranking permeate gap, conductive gap and direct contact MD

2.2.1. Permeate and conductive gap MD

Increasing the gap conductance of PGMD to implement CGMD always results in improved performance. Although increasing the membrane conductivity leads to higher heat conduction loss, the same is not a direct

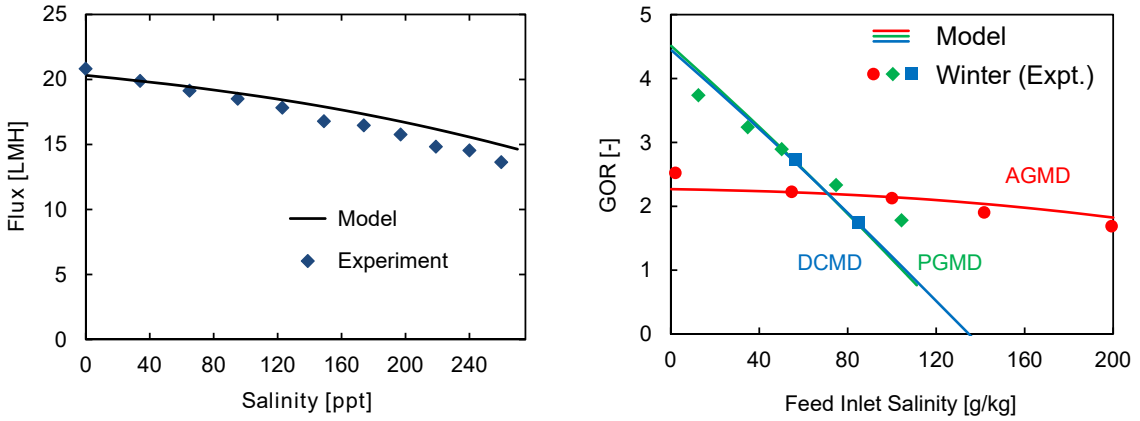

(a) Effect of high salinity on AGMD flux: comparison of experimental results and numerical model predictions.

(b) Comparison of present numerical model with experimental results from large modules reported in Winter [39].

Figure 2: Validation of the finite difference discretized numerical model by comparing against experimental flux data (a) and published energy efficiency data of large-scale modules (b).

outcome of increasing the gap conductivity. In fact, improving the gap's conductance has an effect similar to enhancing the heat transfer coefficients of the feed and cold channels, always resulting in both higher GOR and higher flux, irrespective of the feed salinity. By reducing the non-membrane heat transfer resistances, more of the overall temperature driving force is available across the membrane to produce vapor pressure differences and purified water.

It is important to recognize that PGMD and CGMD designs exist in a continuum: PGMD with a small enough gap thickness can outperform some CGMD implementations. As a result, these configurations can be considered together as permeate or conductive gap MD (P/CGMD), or simply as CGMD, recognizing that the goal is always to design a system with a high gap conductance ($k_{\mathrm{gap}}/d_{\mathrm{gap}}$). Since GOR of CGMD can be several times higher than that of simple PGMD, any additional cost required for modifying the gap design is likely to be justified by the performance improvement.

The potential to increase gap conductance is limited by practical constraints. A lab-bench scale implementation of CGMD could use metal woven mesh spacers, an aluminum foam spacer, a finned condensing plate, or simply reduce the gap thickness down to nearly zero, by using no spacer in the gap and allowing the membrane to be pressed onto the condenser surface. In larger systems, the gap needs to be wide enough to allow permeate flow out of the system without significant pressure build up. A near-zero gap thickness may therefore not be practical.

2.2.2. DCMD: comparison to P/CGMD and the effect of heat exchanger area

In DCMD, the size of the external heat exchanger (HX) relative to the area of MD membrane ($A_{\mathrm{HX}}/A_{\mathrm{m}}$) is a design choice. DCMD is sometimes modeled by setting a fixed terminal temperature difference ($\mathrm{TTD}_{\mathrm{HX}}$)

of the external HX of about 3 °C to ensure a realistic HX size [47]. In Ref. [39], the reported energy efficiency of the experimentally tested DCMD modules was based on assuming an external HX size such that $\mathrm{TTD_{HX}} = 2\,^{\circ}\mathrm{C}$. While DCMD performance was close to that of PGMD, DCMD sometimes outperformed PGMD, but at other times was worse that PGMD. Hence, no clear hierarchy was established. At seawater salinity, and for the other baseline system properties considered in [32], the HX needed seven times the area of the MD membrane for DCMD to match the performance of CGMD ($h_{\mathrm{gap}} = 10^4$ W/m^2·K). On the other hand, even with $A_{\mathrm{HX}} = A_{\mathrm{MD}}$, DCMD outperformed PGMD (with a 1 mm gap, $h_{\mathrm{gap}} = 600$ W/m^2·K).

In fact, the influence of the external HX is very similar to that of the gap: overall system performance improves with an increase in A_{HX} or heat transfer coefficient of the HX (U_{HX}) irrespective of the feed salinity level. Usually, the overall performance of DCMD is predicted by considering the external HX heat transfer separately and solving simultaneously with the MD system heat transfer. When the heat capacity rates of the feed and cold streams are matched at one end of the MD module (as discussed in [40], Appendix A.3), a 'balanced' operating condition results for both the MD module and the external HX. Figure 3 shows that when heat is transferred from a hot stream to a cold stream using two balanced counterflow HXs and an intermediate fluid stream, the overall system can be modeled as one HX whose resistance is equivalent to the resistances of the two individual HXs added in series. (A mathematical proof is given in Appendix A.4).

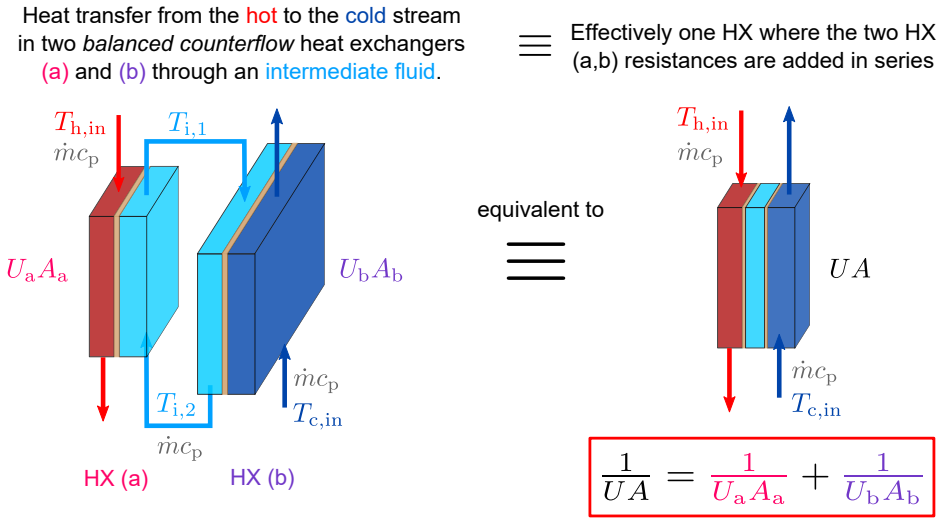

Figure 3: If heat is transfered from a hot fluid to a cold stream using two balanced counterflow heat exchangers, the overall thermal resistance ($1/UA$) is simply the sum of the individual HX resistances. This relates to Fig. 1 (DCMD), where the DCMD module corresponds to HX (a) (on the left) and DCMD's external HX corresponds to HX (b). The intermediate fluid corresponds to the pure water stream in DCMD.

Even though the DCMD module is actually a combined heat and mass exchanger where the flow rates of the two streams change continuously along the module length, the HX analogy model was shown to predict GOR and flux to within about a 10% deviation from 1-D discretized modeling [32] (the impact of this variation in flow rates is small and is discussed below). Consequently, this result for two HXs can be

applied to the DCMD system as well. The external HX thermal resistance can simply be considered in series with the other resistances of the MD module in order to analyze DCMD. While P/CGMD does not have an external HX resistance, DCMD does not have a gap resistance. DCMD has a HX resistance ($1/U_{\mathrm{HX}}A_{\mathrm{HX}}$) in the place of the gap's thermal resistance of P/CGMD ($1/h_{\mathrm{gap}}A_{\mathrm{MD}}$).

The performance of these configurations can therefore be compared based on the magnitude of these thermal resistances. This is validated by plotting the 1-D discretized modeling results for DCMD and CGMD together in Figure 4. Both GOR and flux of CGMD and DCMD are nearly identical (illustrated for two combinations of salinity and system size, $s_{\mathrm{f,in}} = 70$ g/kg, $L = 5$ m and $s_{\mathrm{f,in}} = 200$ g/kg, $L = 2.5$ m) when the gap thermal resistance in CGMD matches the resistance of the HX in DCMD, i.e., $h_{\mathrm{gap}}A_{\mathrm{MD}} = (UA)_{\mathrm{HX}}$.

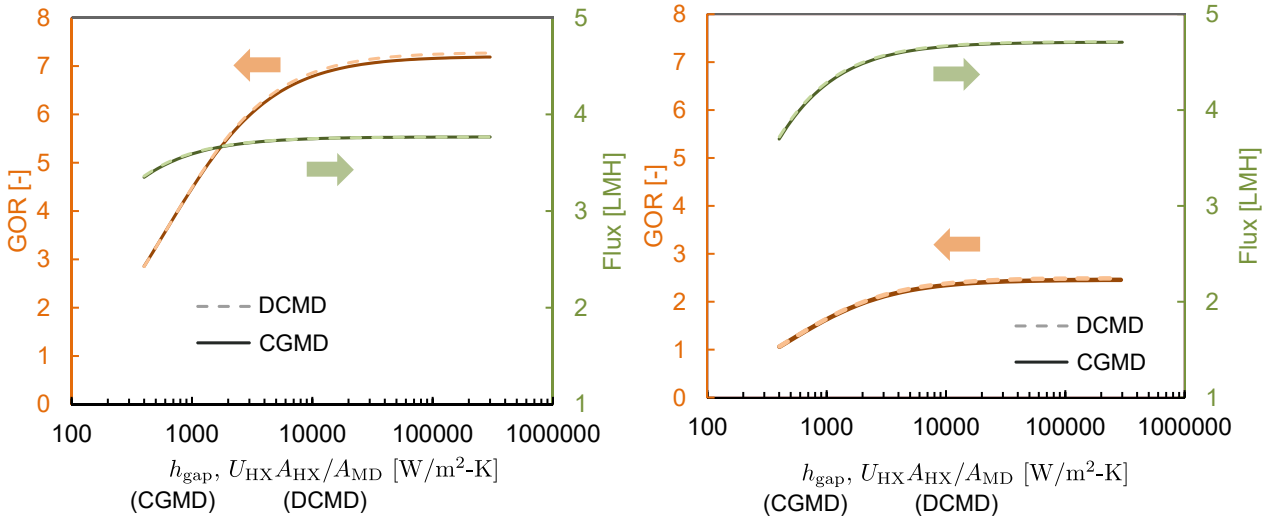

(a) $s_{\mathrm{f,in}} = 70$ g/kg. $L = 5$ m.

(b) $s_{\mathrm{f,in}} = 200$ g/kg. $L = 2.5$ m.

Figure 4: The performance of CGMD and DCMD (using the 1-D model) are similar when the resistance of the gap and the external heat exchanger are matched. $B_0 = 1.8 \times 10^{-10}$ s. Two combinations of feed salinity and system size are shown. Other parameters are fixed at baseline values A.2.

When these thermal resistances are matched, the GOR of DCMD is around 1% higher than that of CGMD because the heat capacity rates of the two streams in the DCMD module do vary along the module length, being highest at the hot end, $\approx \dot{m}_{\mathrm{f,in}}c_{\mathrm{p,f}}$, and declining to $\approx c_{\mathrm{p,f}}\,(\dot{m}_{\mathrm{f,in}} - \dot{m}_{\mathrm{p}})$ at the cold end. In contrast, in the gap MD systems the permeate in the gap along with the feed together constitute one stream of the exchanger, with the preheating stream being the other. As a result, throughout the length of the exchanger, the heat capacity rates are relatively constant, close to the value at the hot-end of the exchanger. The marginally better performance of DCMD is a result of this lower average heat capacity rate, resulting in an improved NTU $= UA/\dot{m}c_{\mathrm{p}}$ and hence higher heat transfer effectiveness ε and GOR. The performance difference is small since the recovery ratio ($= \dot{m}_{\mathrm{p}}/\dot{m}_{\mathrm{f}}$) in a single pass through the MD module is low, $\lesssim 8\%$.

Therefore, the above analysis establishes a general comparison (applicable over a wide range of feed salinities) between P/CGMD and DCMD in terms of the heat transfer resistances. The foregoing analysis

is silent on the relative performance of AGMD compared to these other systems. In the next section, the comparison will be limited to between AGMD and CGMD. Wherever it is not stated explicitly, $h_{\text{gap}} = 10^4$ W/m^2·K is assumed for CGMD.

2.3. Air gap: effectively a thick and insulating membrane

GOR-flux performance curves of AGMD and CGMD are plotted together for two salinity levels in Fig. 5. The relative performance of AGMD and CGMD is more complicated than what was observed among the other configurations. At small area (large flux), CGMD outperforms AGMD irrespective of salinity, whereas at larger system size (and correspondingly higher GOR and lower flux) and particularly at high feed salinity, AGMD outperforms CGMD. The cross-over in performance between AGMD and CGMD happens at higher (and hence more practically relevant) flux levels for higher salinity. The maximum GOR achieved by AGMD is also higher than that of CGMD. These curves are in contrast to the case at seawater salinity, where CGMD outperformed AGMD by about 100% over the entire range of system sizes (or flux levels) considered.

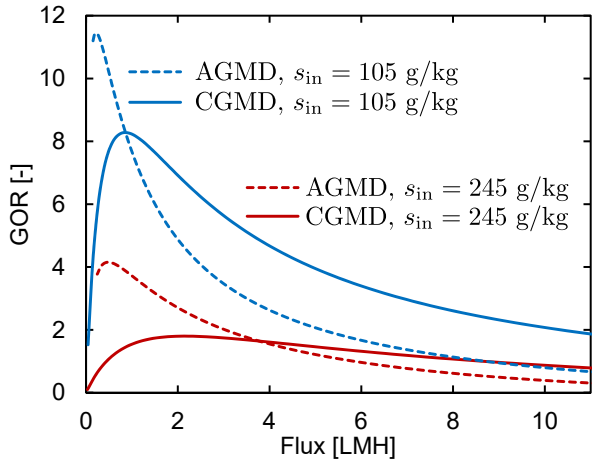

Figure 5: GOR vs. flux curves for AGMD and CGMD at high salinity. At high salinity, AGMD outperforms CGMD at low flux (large system area), and achieves a higher maximum GOR. At $s_{\text{in}} = 245$ g/kg, AGMD performs better energetically even at practically relevant values of flux, 2 to 4 LMH. (System parameters: see Table A.2.)

Note that these results and comparisons are for a relatively thick membrane ($\delta_{\text{m}} = 200$ μm). At lower δ_{m}, the maximum GOR of CGMD would be even lower at high salinity. AGMD on the other hand, would not be affected much since the 1 mm thick air-gap controls the thermal resistance, rather than the membrane thickness, and thus dictates performance.

Figure 6 shows the cross-section of an air gap MD module. In the other MD configurations, water exists on both sides of the membrane and the vapor pressure difference driving flux is related to the temperature and salt concentration of these water streams. In AGMD, the region between the two menisci (salt water meniscus to the left of the membrane and the condensing film surface) can therefore be defined as the effective membrane. In addition to having a thicker 'effective membrane', the overall thermal conductivity ($k_{\text{eff,m}}$)

of this 'membrane' in AGMD is also potentially lower (since the actual membrane material occupies just a small portion of the effective membrane, the remaining being filled with air). If the porosity of the air gap is high, the permeability coefficient (B_0) of this effective membrane would also be higher than that of the membrane. Higher effective membrane thickness δ_{m}, lower membrane effective thermal conductivity $k_{\mathrm{eff,m}}$ and higher permeability coefficient B_0 are all useful in achieving better GOR at high salinity.

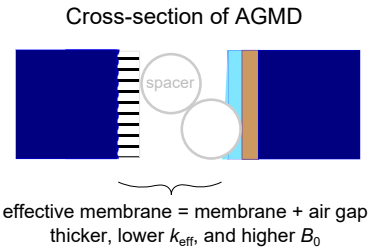

Figure 6: Cross section of AGMD. The air gap along with the membrane can be considered as the effective membrane in the case of AGMD.

One way to match AGMD's high GOR at low flux with CGMD is to use a thick membrane. This suggestion is verified by comparing the performance of AGMD against CGMD with a thick membrane in Fig. 7. When a CGMD system with a thicker membrane is considered (1.2 mm thick, comparable to the combined 1 mm thick air-gap and 0.2 mm thick membrane in AGMD), its GOR-flux profile starts approaching that of AGMD (green curve).

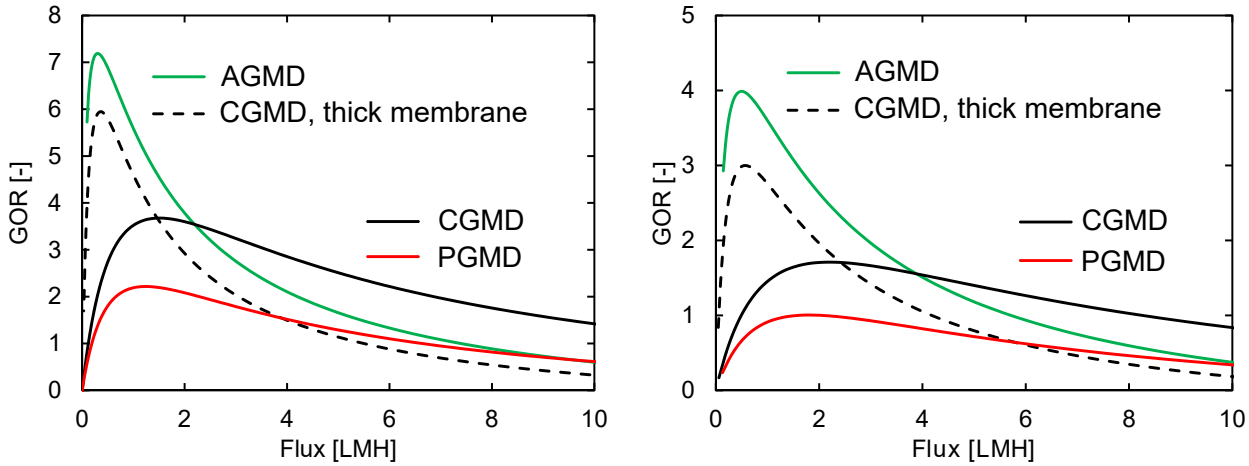

(a) $s_{\mathrm{in}} = 175$ g/kg. $\delta_{\mathrm{m}} = 1.2$ mm for thick CGMD.

(b) $s_{\mathrm{in}} = 250$ g/kg. $\delta_{\mathrm{m}} = 1.2$ mm for thick CGMD.

Figure 7: When the membrane thickness equals the sum of the membrane and air gap thickness of AGMD, performance of CGMD approaches AGMD. AGMD is still better due to lower heat loss across the low thermal conductivity air gap. Lowering the membrane conductivity would make the performance of CGMD with a thick membrane very similar to that of AGMD. CGMD and PGMD with $\delta_{\mathrm{m}} = 0.2$ mm are also shown for comparison. Other system parameters are provided in Table A.2.

At $s_{\mathrm{in}} = 175$ and 250 g/kg, a thick membrane CGMD system performs similar to AGMD (lower GOR

compared to thin-CGMD at high flux and higher GOR at low flux), but its peak GOR is around 10–25% lower than that of AGMD. Specific physical differences account this. The membrane's permeability coefficient was set at 60% of the molecular diffusion upper limit permeability, at $B_0 = 1.5 \times 10^{-10}$ s, in order to account for vapor transport inhibition by the membrane's porosity, and tortuosity. On the other hand, the air gap spacer was considered to have a higher porosity (see Table A.2), and as a result the effective permeability coefficient of the air gap was around $B_{0,\mathrm{air-gap}} \approx 2.15 \times 10^{-10}$ s. Similarly, the effective conductivity of the air gap was set at 0.032 W/m·K compared to $k_{\mathrm{eff,m}} = 0.062$ W/m·K. Therefore, $B_0/k_{\mathrm{eff,m}}$ was higher for the effective membrane of AGMD, resulting in higher maximum GOR of AGMD compared to CGMD with a thick membrane.

With the development of ultra-porous MD membranes with enhanced vapor permeability and much lower thermal conductivity [51], this disadvantage of thick-CGMD compared to AGMD at high salinity and low flux can be bridged. This development is particularly important since AGMD with small gap thickness can get partially flooded, pushing AGMD's performance below that of even thin-CGMD towards PGMD (red curve in Fig. 7). The practical implications of these effects on the choice of MD configuration for high salinity are summarized in Section 2.5.

2.4. Choosing MD membrane thickness

Making a more permeable or less thermally conductive membrane (to increase $B_0/k_{\mathrm{eff,m}}$) is contingent on developing novel membrane fabrication methods. On the other hand, the thickness of the membrane can be adjusted as an independent parameter during fabrication. We have shown that AGMD is better for low flux and high salinity, whereas CGMD is better at high flux and low salinity. Since AGMD-type performance can be obtained by using thicker membranes in CGMD, this section focuses on the choice of optimal membrane thickness for a CGMD system.

The ideal membrane thickness depends not only the feed water salinity, but also on the flux at which the system operates. Figure 8 shows GOR vs. flux curves for a three membrane thicknesses. At high flux, the thicker membranes have a lower GOR compared to thinner membranes, whereas at low flux, the thicker membranes achieve higher GOR. At each flux, there exists an optimum thickness. The overall best-case (upper limit GOR) curve, when δ_{m} is allowed to vary, is tangent to each of the GOR-flux curves obtained at fixed δ_{m}. This resulting curve is shown as a solid line in Fig. 8.

Similar upper limit curves can be obtained for each salinity based on the same procedure and are plotted in Fig. 9a. Correspondingly, the optimal membrane thickness as a function of flux is shown in Fig. 9b. These curves are valid for the baseline channel properties listed in Table A.2.

Figures 9a and 9b together can be used to pick the optimal membrane thickness for a given application (defined by s_{in}, C_{GOR} and C_{Flux}). First, Fig. 9a is used to pick an operating point along the max. GOR-flux operating curve to minimize specific cost (Eq. A.5). The location of the optimum point is a function of the relative specific cost of thermal energy and amortized system size ($C_{\mathrm{GOR}}/C_{\mathrm{flux}}$). At the baseline

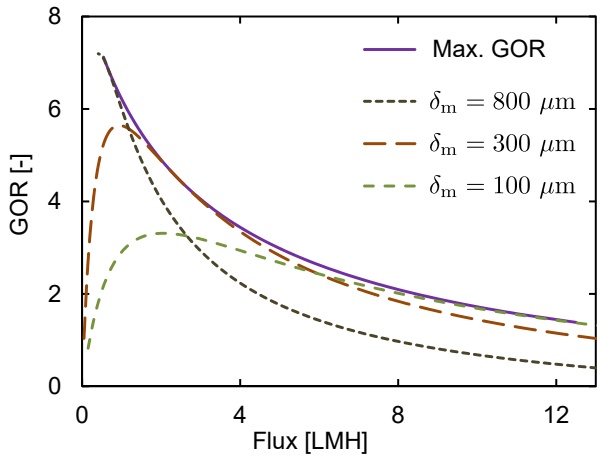

Figure 8: GOR vs. flux at various membrane thicknesses for CGMD at $s_{in} = 150$ g/kg. For each flux, GOR is maximized at a specific value of membrane thickness δ_m. The solid curve is the locus of maximum GOR values, calculated by allowing the membrane thickness to vary.

condition defined in Appendix A.1 this ratio is 22.6. If the present cost of natural gas is considered, or if the system capital cost is higher, this ratio would be lower. Once this operating point is identified, the required membrane thickness can be obtained at the same value of flux from Fig. 9b. Representative results are shown for three values of the cost ratio.

2.5. Practical implications for choice of MD configuration

Figure 10 shows the approximate external area required for DCMD to achieve the same GOR as a CGMD system, which defined by its gap conductance. The following conditions were considered in Ref. [32]: $h_{gap} = 10^4$ W/m^2·K, and $U_{HX} = 1300$ W/m^2·K. Numerical modeling of the full systems showed that the DCMD HX had to be about 7 times the size of the membrane to match the GOR of the CGMD system. DCMD with $A_{HX} = A_m$ was also found to outperform PGMD (with $h_{gap} = 600$ W/m^2·K). Similar conclusions can be drawn without full modeling from Figure 10. In Winter [39], since TTD is fixed, $(UA)_{HX}$ changes with changes in feed flow rate. As a result, in some cases $(UA)_{HX}$ is larger than $h_{gap}A_{MD}$, resulting in DCMD's better performance compared to PGMD, whereas in other cases the opposite was true.

Since DCMD and P/CGMD are essentially equivalent in terms of their overall performance, the choice among these configurations is only a function of economics: the configuration with a lower C_{flux} for the same performance is preferred. Based on Fig. 10, for a 0.5 mm gap width and $k_{eff,m} = 3$ W/m·K in CGMD, the area of the HX in DCMD ($U_{HX} = 1300$ W/m^2·K) has to be about 4.5 times that of the condenser surface area in CGMD. The amount of metal required to increase the conductance of the thin gap in CGMD is likely to be lower than what is needed for the larger external HX, in addition to other advantages of CGMD such as having only one flow loop and a lower pumping power consumption. Based on these factors, CGMD would likely be a cheaper system to implement for the same overall performance.

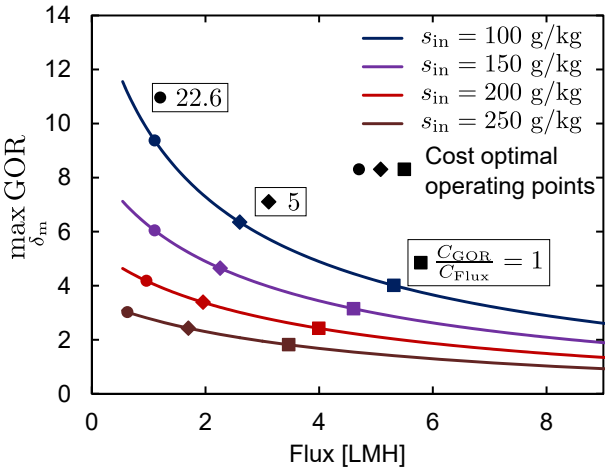

(a) Maximum GOR is plotted as function of flux. At each flux, the system is designed at the membrane thickness that maximizes GOR.

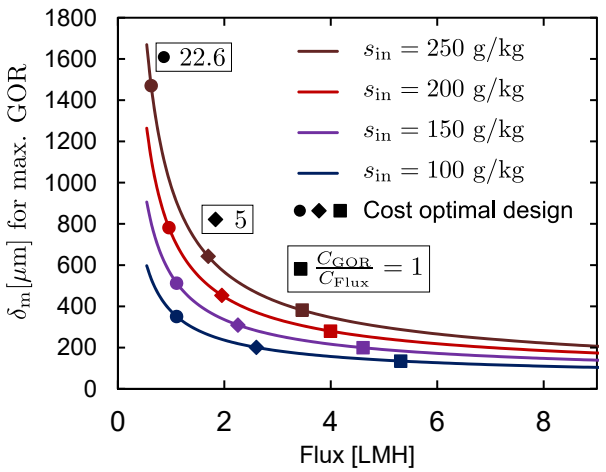

(b) The thickness at which energy efficiency is maximized for CGMD as a function of flux.

Figure 9: Charts for choosing membrane thickness and system size: maximum GOR and the thickness at which GOR is maximized are plotted as a function of flux. At the known feed salinity, a point along the max-GOR vs. flux graph is chosen to minimize the cost of water. Once this operating point is chosen, the corresponding value of membrane thickness can be obtained from Fig. 9b. Representative choices of optimal system design are shown for three values of C_{GOR}/C_{flux} [L/m^2·hr].

AGMD is particularly promising at high feed salinities. But a thin air gap (less than about 1 mm) can get partially or completely flooded during operation (Fig. 11). Recent visualizations [52, 53] of the condensation process within the air gap have confirmed that the film is affected by the gap spacer and is quite different from the ideal case depicted Fig. 6. In Appendix A.5 the susceptibility of large area systems to gap flooding is highlighted. Such flooding would lead to a shift in AGMD performance towards that of PGMD (red curves in Fig. 7), which is particularly bad at high salinity.

Since CGMD and DCMD systems with thick membranes perform similar to AGMD, while eliminating the danger of air-gap flooding and PGMD type operation, these designs may be more robust alternatives to AGMD. This advantage will be more pronounced once ultra-porous membranes are commercially available, since at present an ideal AGMD system outperforms CGMD with a thick membrane. These results assume that high h_{gap} or $(UA)_{HX}$ can be implemented, since the equivalent resistance in AGMD (of the thin film condensate) is small. Figure 11 shows the overall comparison between various options at high salinity.

3. Part 2: Deriving general results for sizing MD systems

3.1. Methodology: simplified heat exchanger (HX) analogy model adapted to high salinity

A simplified model of MD will be used for deriving generalized results for sizing MD systems. This model, which does not employ length-wise discretization, is based on an analogy to heat exchanger analysis using the ε-NTU method, and was proposed previously by the present authors [32] and will be used to derive

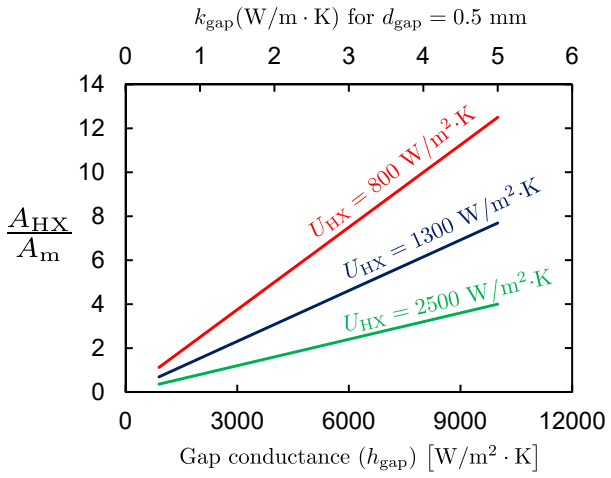

Figure 10: The relative size of HX in DCMD to match a CGMD system's GOR.

generalized results for sizing MD systems. (Similar concepts have been developed for modeling a variety of pressure-driven osmotic mass exchangers [54, 55, 56, 57]; and simplified models based on the ε-NTU method have also been applied for predicting DCMD flux [58].) We refer to this approach as the HX analogy model. This model has previously been applied to PGMD, CGMD, and DCMD at seawater salinity. Based on the results of Part 1, the previously proposed models are generalized as one model for all single stage MD configurations, and the model applicability is also extended to higher feed salinity.

The corresponding MD resistance network is shown in Fig. 12. In the 1-D discretized model, the variation of the membrane's vapor transfer resistance ($R_{m,vapor}$), which is lowest at the high temperature end of the module, is captured. On the other hand, in the HX analogy model, $R_{m,vapor}$ is averaged over length. As a result, all the heat transfer resistances are constant over the exchanger length, just as in a simple HX model. In addition to varying locally, $R_{m,vapor}$ is also affected by system size: it is higher for larger systems. The effect of module length on the magnitude of $R_{m,vapor}$ is still captured, through ΔT_m, the average temperature drop across the membrane. A larger MD system results in a lower terminal temperature difference (TTD) and ΔT_m, hence resulting in a higher vapor transfer resistance across the membrane (the equation for h_m^{mass} given in Fig. 12, as derived in [32]).

In this simplified model, the effect of dissolved salt on vapor pressure depression and on feed solution specific heat are included in order to extend the applicability of this model to high salinity. The effect of salinity on the vapor pressure of the feed stream is incorporated through ΔT_{VPD}, the vapor pressure depression temperature (which is approximately equal to the boiling point elevation or ΔT_{BPE}). Here, ΔT_{VPD} is defined so that the vapor pressure of a saline feed solution at temperature T_f and salinity s_f is equal to the saturation vapor pressure of pure water at a lower temperature, $T = T_f - \Delta T_{VPD}(T_f, s_f) \approx T_f - \Delta T_{BPE}(T_f, s_f)$. Refer to Appendix A.6 for a discussion of this concept. Here, ΔT_{VPD} is evaluated at the mean temperature and at a salinity 4% higher than the inlet feed stream (to account for feed concentration increase with length and concentration polarization. Concentration polarization can be modeled in more detail as a function of

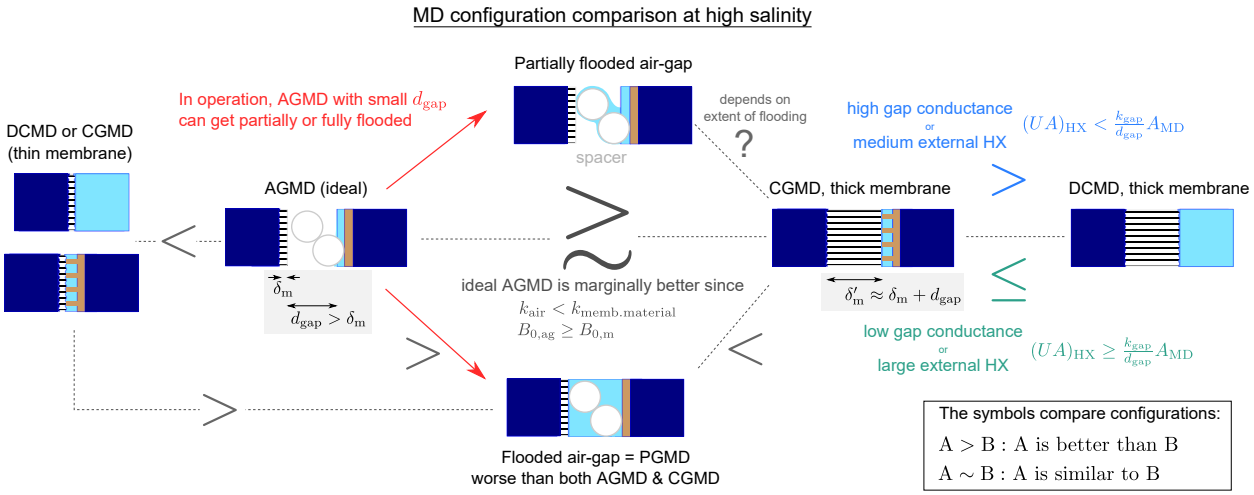

Figure 11: Relative performance relationships between various MD configuration at high salinity. A < B and A > B are used to indicate that performance of system A is worse or better than that of system B. An ideal AGMD system is optimal (2nd from left), if flooding can be prevented. If not, CGMD with a thick membrane (2nd from right) is almost as good, while being more robust.

flux and channel mass transfer coefficient if better accuracy is desired at high flux).

Once this resistance network is established, an overall heat transfer coefficient (U, for UA the reciprocal of total resistance) can be determined, from which NTU $= UA/\dot{m}c_p$ is found. NTU is a non-dimensional measure of system area. Exchanger effectiveness can be evaluated as $\varepsilon = \text{NTU}/(1 + \text{NTU})$ for balanced counterflow MD systems [59] (See Appendix A.3 for a brief overview of balancing flows in MD systems). η is determined based on the ratio of membrane resistances to heat transfer mediated by vapor transport and heat conduction. GOR is then estimated as $\eta \cdot \varepsilon/(1-\varepsilon)$ or equivalently,

$$\text{GOR} = \eta\,\text{NTU} \tag{5}$$

3.2. Design goals based on the resistance network model

Three key goals for MD system design are described below:

1. A low total resistance (high overall heat transfer coefficient U) is ideal, so that for the same area A, NTU and therefore heat transfer effectiveness ε are increased.
2. To achieve, a high GOR, η should also be high, in addition to ε: most of the energy transfer across the membrane should be mediated by vapor transport, ideally with very little heat conduction loss. Correspondingly, the ratio of membrane conduction resistance to the resistance to vapor transport, $\phi_{c:v}$, should be high:

$$\begin{aligned}\phi_{c:v} &= \frac{R_{\text{memb. conduction}}}{R^{\circ}_{\text{memb. vapor}}} \\ &= \frac{B_0}{k_{\text{eff,m}}} h_{fg}\,\text{bA}e^{\text{b}T_{p,avg}}\end{aligned} \tag{6}$$

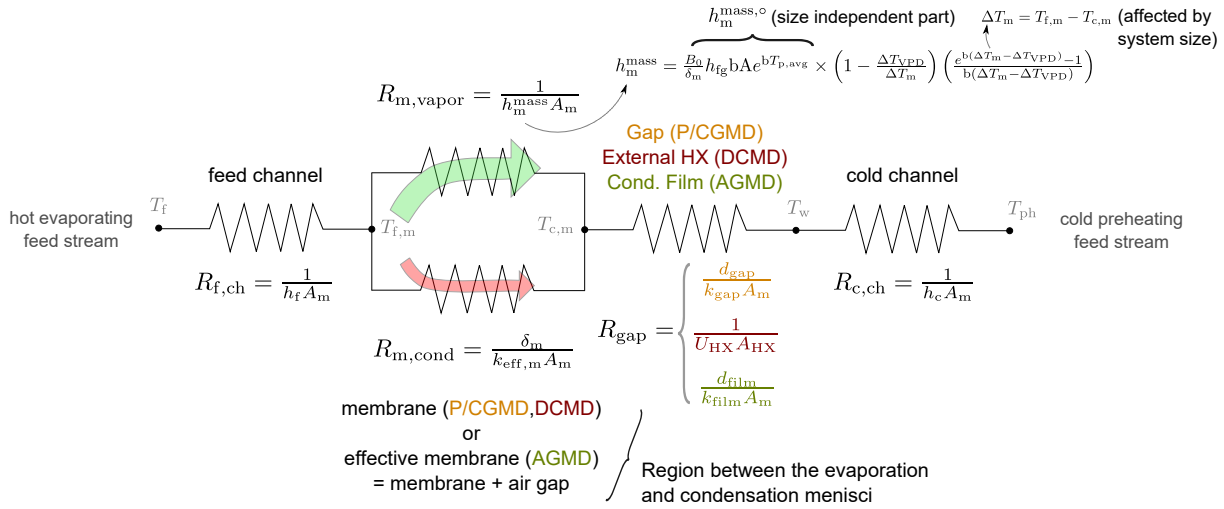

Parameters defining general MD system		Design goals:
Resistance Ratios	$\frac{\text{conduction}}{\text{vapor}^\circ} = \phi_{c:v} = \frac{R_{m,cond}}{R^\circ_{m,vapor}}$	Maximize
	$\frac{\text{channels}}{\text{memb cond.}} = \phi_{ch:m} = \frac{R_{channels}}{R_{m,cond}}$	Minimize
Non-membrane thermal resistances	where, $R_{channels} = R_{f,ch} + R_{gap} + R_{c,ch}$	Minimize
System size	$NTU = \frac{UA}{\dot{m} c_p} = \frac{T_{ph,out} - T_{ph,in}}{T_{f,in} - T_{ph,out}}$	$NTU < NTU^{crit}(\phi_{ch:m}, \phi_{c:v}, s_f)$ (necessary condition)
Membrane thickness	δ_m	For fixed $R_{channels}, \phi_{c:v}$ cost optimal δ_m and system size as a function of C_{GOR}/C_{flux}

Figure 12: Updated resistance network model of general single-stage MD system. The design goals are summarized.

where A = 1054.8 Pa and b = 0.0479 °C^{-1} are obtained by fitting data to $P_{\text{sat}}(T) = \text{A}e^{\text{b}T}$. $k_{\text{eff,m}}$ is the effective thermal conductivity of the membrane, and is influenced by the conductivity of the membrane material (k_{m}) as well porosity, tortuosity and geometry of the pores. Even if the membrane material is eliminated (porosity $\phi_{\text{m}} = 1$), vapor would still conduct some heat; hence, in practice the heat conduction loss is always non-zero.

Note that $\phi_{\text{c:v}}$ is defined to be independent of system size (i.e., independent of ΔT_{m}) by considering $h_{\text{m}}^{\text{mass},0}$ (see Fig. 12) instead of the total conductance due to vapor mass transport, $h_{\text{m}}^{\text{mass}}$. Also, $\phi_{\text{c:v}}$ is independent of membrane thickness because it cancels from the ratio of vapor permeability ($B = B_0/\delta_{\text{m}}$) and heat conductance ($h_{\text{cond,memb}} = k_{\text{eff,m}}/\delta_{\text{m}}$). Stated another way, $\phi_{\text{c:v}}$ is the non-dimensional ratio of membrane's vapor permeability coefficient to its effective thermal conductivity.

3. To achieve a high flux and high GOR, the temperature difference across the membrane (ΔT_{m}) should be as close as possible to the terminal temperature difference (TTD) or the temperature difference between the bulk streams (ΔT_{b}). A temperature difference across the membrane drives pure water production, but temperature drops across the other thermal resistances are simply losses of the available driving temperature difference between the hot and cold bulk streams, ΔT_{b}. As a result, in an efficient MD system, ΔT_{m} must be close to ΔT_{b}.

$$\frac{\Delta T_{\text{m}}}{\Delta T_{\text{b}}} = \frac{R_{\text{membrane}}}{R_{\text{total}}} = \frac{1}{1 + \phi_{\text{ch:m}}\left[1 + \phi_{\text{c:v}}\left(1 - \frac{\Delta T_{\text{VPD}}}{\Delta T_{\text{m}}}\right)\left(\frac{e^{b(\Delta T_{\text{m}} - \Delta T_{\text{VPD}})} - 1}{b(\Delta T_{\text{m}} - \Delta T_{\text{VPD}})}\right)\right]} \tag{7}$$

where, for CGMD,

$$\begin{aligned}\phi_{\text{ch:m}} &= \frac{\Sigma R_{\text{non-membrane,i}}}{R_{\text{memb. conduction}}} \\ &= \frac{\frac{1}{h_{\text{f}}} + \frac{1}{h_{\text{c}}} + \frac{d_{\text{gap}}}{k_{\text{gap}}}}{\frac{\delta_{\text{m}}}{k_{\text{eff,m}}}}\end{aligned} \tag{8}$$

For ΔT_{m} to be close to ΔT_{b}, $\phi_{\text{ch:m}}$, the ratio of the total resistance of non-membrane channels to the conduction resistance of the membrane, should be as low as possible.

Like $\phi_{\text{c:v}}$, $\phi_{\text{ch:m}}$ is also defined to be independent of system size. A low value of $\phi_{\text{ch:m}}$ can be achieved by increasing the heat transfer coefficients of the hot and cold channels or the gap region. Note that, unlike $\phi_{\text{c:v}}$, $\phi_{\text{ch:m}}$ is not independent of membrane thickness. A low value of $\phi_{\text{ch:m}}$ can also be achieved by making the membrane thicker (or otherwise increasing the membrane's conduction resistance).

These parameters can be used to understand the general design goals for improving MD performance. The importance of the two resistance ratios (similar to $\phi_{\text{c:v}}, \phi_{\text{ch:m}}$) as well as of the temperature-difference ratio $\Delta T_{\text{m}}/\Delta T_{\text{VPD}}$ was brought out very clearly by Bandini et al. [60], in the context of small-area DCMD system design.

The resistance network can be completely defined by one of the resistance terms (e.g., $\Sigma R_{\text{non-membrane,i}}$), and the two non-dimensional ratios defined above. GOR, which is non-dimensional, can actually be expressed as a function of only the two non-dimensional resistance ratios and the dimensionless system size, expressed

as NTU, independent of the magnitudes of the individual resistances. This fact will be used to derive a general expression for the critical system size in Section 3.3.

Unlike GOR, flux is a dimensional quantity and is affected by the magnitude of the resistances in addition to resistance ratios. At the same values of $\phi_{\mathrm{c:v}}, \phi_{\mathrm{ch:m}}$, a high overall U is preferable in order to achieve better GOR-flux performance. While $\phi_{\mathrm{ch:m}}$ can be reduced by increasing the membrane thickness, this approach is less desirable than reducing the resistance of the non-membrane regions, as shown in Appendix A.7.

The optimal MD membrane has already been recognized to be that which maximizes $\phi_{\mathrm{c:v}}$. This parameter is defined independent of membrane thickness. As a result, the optimal method to achieve any given membrane thickness is using an air-gap, with a very thin physical membrane, provided gap flooding is not a concern. Further improvements in $\phi_{\mathrm{c:v}}$ can be achieved through methods such as partial evacuation of the air gap [39, 61], which help both increase B_0 as well as reduce $k_{\mathrm{eff,m}}$. In this manner, a partially evacuated air gap can also be incorporated into this analytical framework.

Once all these techniques are used to maximize $\phi_{\mathrm{c:v}}$, from the system design perspective, the heat transfer coefficients of all the non-membrane portions of the system should be maximized. The extent to which these can be increased is limited by cost constraints. For a given set of non-membrane thermal resistances, the optimal membrane thickness and system size can then be determined based on the method proposed in Section 2.4. These design goals are also described in Fig. 12.

3.3. Evaluating critical system size as a function of heat transfer resistances

3.3.1. Systems larger than a critical size must be avoided

For a zero salinity feed stream, the thermodynamic maximum GOR is ∞. In other words, the thermodynamic least energy required to create pure water from already pure water is 0. With a membrane distillation system, this situation is realized when $A_{\mathrm{MD}} \to \infty$, which correspondingly leads to $J \to 0$. For non-zero feed salinity, the thermodynamic maximum GOR can be expressed as $\mathrm{GOR}_{\mathrm{max,MD}} = \frac{T_{\mathrm{f,in}} - T_{\mathrm{c,in}}}{\Delta T_{\mathrm{VPD}}(T_{\mathrm{f,in}}, s_{\mathrm{f,in}})} - 1$ [32]. This cannot be achieved in real MD systems since the membrane would have to be perfectly insulating, wherein even the vapor does not conduct any heat from the feed side to the cold side ($\phi_{\mathrm{c:v}} \to \infty$).

For real membranes, thermal efficiency $\eta \neq 1$, and η decreases with an increase in system size, as ΔT_{m} decreases and approaches ΔT_{VPD}. In fact, beyond a certain 'critical system size', the rate of decrease of η is faster than the increase in $\varepsilon/(1-\varepsilon)$, leading to a net decline in $\mathrm{GOR} = \eta \cdot \varepsilon/(1-\varepsilon)$. This corresponds to the peak GOR at low flux observed in Fig. 7. While flux keeps decreasing with a further increase in system size, beyond the critical system size, GOR also starts declining rather than improving. As a result, there is no rationale for designing or operating an MD system under this unfavorable condition.

3.3.2. Deriving a closed-form expression for critical system size

The goal of this section is to derive a generally applicable expression for critical system size, using the non-dimensional parameters from the simplified HX analogy framework. First, from Eq. 5, $\mathrm{GOR} = \eta \times \mathrm{NTU}$, where $\mathrm{NTU} = UA/\dot{m}c_{\mathrm{p}}$. Note that since the overall heat transfer coefficient U is a function of system size

(since ΔT_{m} decreases with increasing area, resulting in a lower $h_{\mathrm{m}}^{\mathrm{mass}}$), NTU is not a linear function of system size.

Figure 13 shows GOR as a function of NTU for various feed salinity levels (for baseline values of $\phi_{\mathrm{c:v}}, \phi_{\mathrm{ch:m}}$). The dotted lines are from the simplified HX analogy model of MD. Note that the HX analogy model is able to effectively capture the GOR vs. NTU curves, including the peak GOR and critical system NTU at which GOR reaches a maximum. For pure water, GOR continuously increases with an increase in system size; GOR has no thermodynamic upper limit in this case. This is a result of η remaining relatively unchanged (for pure feed) as the driving temperature difference across the membrane ΔT_{m} decreases. Experimentally, an equivalent result was observed for η as a function of membrane thickness in DCMD; even at small membrane thickness (corresponding to small ΔT_{m}), η does not decline for a pure feed [27, 45].

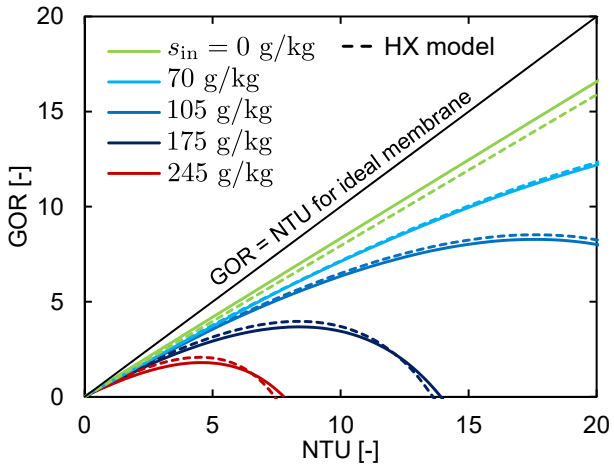

Figure 13: Energy efficiency (GOR) is plotted against NTU (dimensionless system size) to show the existence of a critical size ($\mathrm{NTU}^{\mathrm{crit}}$) beyond which GOR decreases. The operating conditions should always be to the left of this maximum GOR point. Dotted lines indicate results from the simplified HX analogy model, and demonstrate that the peak is captured quite well by the simplified HX model as well. System parameters: Table A.2.

At high feed salinity, although effectiveness ε increases as system size increases, η decreases due to a decrease in the flux-driving temperature difference. The HX model represents η as:

$$\eta = \frac{1}{1 + \left[\phi_{\mathrm{c:v}} \left(1 - \frac{\Delta T_{\mathrm{VPD}}}{\Delta T_{\mathrm{m}}}\right) \left(\frac{e^{b(\Delta T_{\mathrm{m}} - \Delta T_{\mathrm{VPD}})} - 1}{b(\Delta T_{\mathrm{m}} - \Delta T_{\mathrm{VPD}})}\right)\right]^{-1}} \tag{9}$$

NTU can be expressed as a function of $\phi_{\mathrm{c:v}}$, $\phi_{\mathrm{ch:m}}$, ΔT_{m}, and salinity (through ΔT_{VPD}) as:

$$\mathrm{NTU} = \frac{\Delta T_{\mathrm{max}}}{1 + \phi_{\mathrm{ch:m}} + \phi_{\mathrm{ch:m}}\phi_{\mathrm{c:v}} \left(1 - \frac{\Delta T_{\mathrm{VPD}}}{\Delta T_{\mathrm{m}}}\right) \left[\frac{e^{b(\Delta T_{\mathrm{m}} - \Delta T_{\mathrm{VPD}})} - 1}{b(\Delta T_{\mathrm{m}} - \Delta T_{\mathrm{VPD}})}\right]} - 1 \tag{10}$$

Putting Eqs. 9 and 10 together, GOR can be expressed as a function of $\phi_{\mathrm{ch:m}}$, $\phi_{\mathrm{c:v}}$, ΔT_{VPD}, ΔT_{m}, and

$\Delta T_{\max} = T_{\mathrm{f,in}} - T_{\mathrm{c,in}}$:

$$\mathrm{GOR} = \frac{\frac{\Delta T_{\max}}{1+\phi_{\mathrm{ch:m}}+\phi_{\mathrm{ch:m}}\phi_{\mathrm{c:v}}\left(1-\frac{\Delta T_{\mathrm{VPD}}}{\Delta T_{\mathrm{m}}}\right)\left[\frac{e^{b(\Delta T_{\mathrm{m}}-\Delta T_{\mathrm{VPD}})}-1}{b(\Delta T_{\mathrm{m}}-\Delta T_{\mathrm{VPD}})}\right]} - 1}{1+\left[\phi_{\mathrm{c:v}}\left(1-\frac{\Delta T_{\mathrm{VPD}}}{\Delta T_{\mathrm{m}}}\right)\left(\frac{e^{b(\Delta T_{\mathrm{m}}-\Delta T_{\mathrm{VPD}})}-1}{b(\Delta T_{\mathrm{m}}-\Delta T_{\mathrm{VPD}})}\right)\right]^{-1}} \tag{11}$$

Table 1 summarizes the practical significance of the generalized non-dimensional and other parameters.

Table 1: List of system variables and non-dimensional parameters used to characterize MD system critical size.

System variables	Dimensionless parameter	Summary
L, $\dot{m}_{\mathrm{f,in}}$	NTU	Defines system size. L is physical length of the module in the flow direction. NTU $= \frac{U\times(Lw)}{\dot{m}c_{\mathrm{p}}}$. NTU is not a linear function of L since $U = f(L)$. Membrane mass transfer coefficient ($h_{\mathrm{m}}^{\mathrm{mass}}$) is a function of ΔT_{m}, which decreases at larger L. Experimentally NTU can be inferred as NTU $= \frac{T_{\mathrm{c,out}}-T_{\mathrm{c,in}}}{\mathrm{TTD_{MD}}}$.
δ_{m}, $h_{\mathrm{f}}, h_{\mathrm{c}}, h_{\mathrm{gap}}$	$\phi_{\mathrm{ch:m}}$	Ratio of combined resistance of non-membrane sections to membrane conduction resistance. $\phi_{\mathrm{ch:m}}$ increases for a thinner membrane or at higher channel heat transfer coefficients.
B_0, $k_{\mathrm{eff,m}}$, $T_{\mathrm{p,avg}}$	$\phi_{\mathrm{c:v}}$	Ratio of the membrane conductance resistance to (size independent part of) membrane mass transfer resistance. A higher value is better. $\phi_{\mathrm{c:v}}$ can be increased by increasing B_0 or reducing $k_{\mathrm{eff,m}}$.
ΔT_{VPD}, $s_{\mathrm{f,in}}$	-	ΔT_{VPD}, which is approximately equal to the boiling point elevation, is a measure of the vapor pressure depression of the saline solution. It is a function feed salinity and average temperature. For NaCl solutions, as feed salinity increases up to saturation at 260 g/kg, ΔT_{VPD} increases to around 6 °C.
$\Delta T_{\max} = T_{\mathrm{f,in}} - T_{\mathrm{c,in}}$	-	This is fixed at 60 °C in this study: $T_{\mathrm{f,in}} = 85\,^{\circ}\mathrm{C}$, $T_{\mathrm{f,in}} = 25\,^{\circ}\mathrm{C}$. At lower top temperature, in addition to adjusting $\Delta T_{\max}$, the effect of lower temperature on B_0 should also be accounted for.

As described previously, ΔT_{m} decreases with an increase in system size and can be taken as a proxy for system size in the GOR expression, Eq. (11). The critical system size ($\mathrm{NTU}^{\mathrm{crit}}$ or L^{crit}), above which

MD systems should not be operated, can be evaluated by finding the corresponding $\Delta T_{\mathrm{m}}^{\mathrm{crit}}$, below which the system should not be operated. GOR reaches a maximum at this critical system size (see Fig. 13). Near the peak GOR, $\Delta T_{\mathrm{m}} \approx \Delta T_{\mathrm{VPD}}$, so $\frac{e^{b(\Delta T_{\mathrm{m}}-\Delta T_{\mathrm{VPD}})}-1}{b(\Delta T_{\mathrm{m}}-\Delta T_{\mathrm{VPD}})} \approx 1$. Hence, the GOR expression can be simplified to:

$$\mathrm{GOR} \approx \frac{\frac{\Delta T_{\mathrm{max}}}{1+\phi_{\mathrm{ch:m}}+\phi_{\mathrm{ch:m}}\phi_{\mathrm{c:v}}\left(1-\frac{\Delta T_{\mathrm{VPD}}}{\Delta T_{\mathrm{m}}}\right)}-1}{1+\left[\phi_{\mathrm{c:v}}\left(1-\frac{\Delta T_{\mathrm{VPD}}}{\Delta T_{\mathrm{m}}}\right)\right]^{-1}} \tag{12}$$

By setting $\frac{\partial \mathrm{GOR}}{\partial \Delta T_{\mathrm{m}}}=0$, $\Delta T_{\mathrm{m}}^{\mathrm{crit}}$ can be expressed as an explicit function of $\phi_{\mathrm{ch:m}}$, $\phi_{\mathrm{c:v}}$, ΔT_{VPD} and ΔT_{max}:

$$\Delta T_{m}^{\mathrm{crit}} = \Delta T_{\mathrm{VPD}} \cdot \phi_{\mathrm{ch:m}} \left[\frac{\Delta T_{\mathrm{max}} + \phi_{\mathrm{c:v}}\left(\Delta T_{\mathrm{max}} + \phi_{\mathrm{ch:m}} \cdot \Delta \mathrm{T}_{\mathrm{VPD}}\right) + \sqrt{\frac{\Delta T_{\mathrm{max}}(1+\phi_{\mathrm{ch:m}})[\Delta T_{\mathrm{max}}+\phi_{\mathrm{c:v}}(\Delta T_{\mathrm{max}}-\Delta T_{\mathrm{VPD}})]}{1+\phi_{\mathrm{ch:m}}(1+\phi_{\mathrm{c:v}})}}}{\left(\Delta T_{\mathrm{max}} + \phi_{\mathrm{ch:m}} \cdot \Delta T_{\mathrm{VPD}}\right)\left[1+\phi_{\mathrm{ch:m}}\left(1+\phi_{\mathrm{c:v}}\right)\right] - \Delta T_{\mathrm{max}}} \right] \tag{13}$$

The $\mathrm{NTU}^{\mathrm{crit}}$ at which GOR is maximized can in turn be obtained by plugging $\Delta T_{\mathrm{m}}^{\mathrm{crit}}$ into Eq. 10. $\mathrm{NTU}^{\mathrm{crit}}$ as a function of $\phi_{\mathrm{ch:m}}$, $\phi_{\mathrm{c:v}}$ and salinity is plotted in Fig. 14.

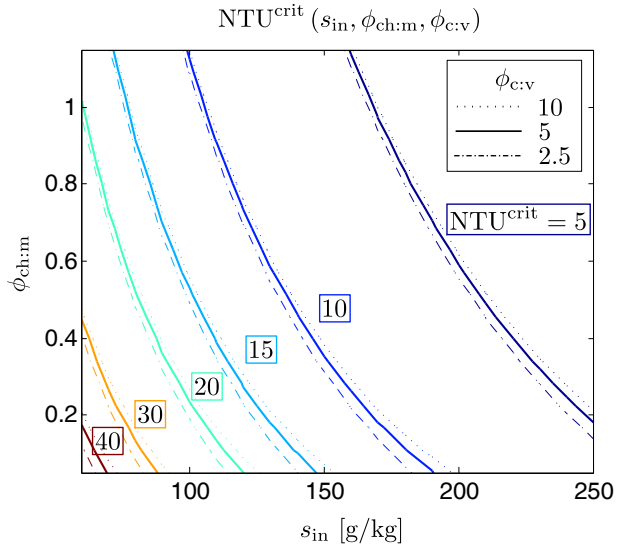

Figure 14: Level curves of critical dimensionless system size $\mathrm{NTU}^{\mathrm{crit}}$ as a function of $\phi_{\mathrm{ch:m}}$ (ratio of the channels' thermal resistance to membrane conduction resistance), salinity, and $\phi_{\mathrm{c:v}}$ (non-dimensional ratio of membrane vapor permeability to thermal conductivity). Design and operation should be selected to ensure $\mathrm{NTU} < \mathrm{NTU}^{\mathrm{crit}}$.

The NTU of a system in operation can be inferred based on temperature measurements. Applying energy balance on the preheat stream, $UA\Delta T_{\mathrm{b}} = \dot{m} c_p \Delta T_{\mathrm{ph,axial}}$, where ΔT_{b} is the temperature difference between the feed and cold bulk temperatures, and $\Delta T_{\mathrm{ph,axial}}$ is the temperature difference along the length of the cold channel. Rearranging, $\mathrm{NTU} = \frac{\Delta T_{\mathrm{ph,axial}}}{\Delta T_{\mathrm{b}}} \approx \frac{T_{\mathrm{ph,out}}-T_{\mathrm{ph,in}}}{T_{\mathrm{f,in}}-T_{\mathrm{ph,out}}}$. These temperatures can be readily measured for an MD module in operation to infer its NTU in order to ensure operation at $\mathrm{NTU} < \mathrm{NTU}^{\mathrm{crit}}$.

$\mathrm{NTU}^{\mathrm{crit}}$ as a non-dimensional parameter is useful when a system is operating, and inlet and outlet temperatures can be measured. For designing a system, however, the more relevant parameter is the critical length of the module. This critical length can be represented as a function of feed salinity, and non-

dimensional parameters $\phi_{\text{ch:m}}$ and $\phi_{\text{c:v}}$ as shown in Fig. 15. The dimensional critical length also depends on the actual resistance within the module, in addition to the dimensionless resistance ratios.

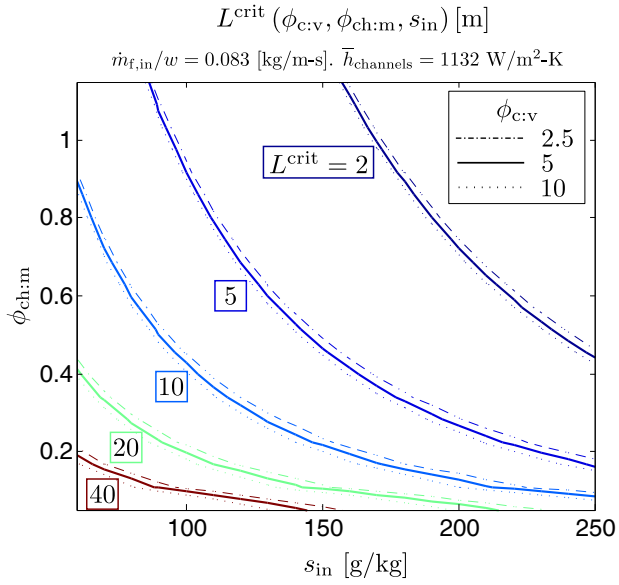

Figure 15: Level curves of critical length L^{crit} (in meters) as a function of salinity and the dimensionless ratios $\phi_{\text{ch:m}}$ and $\phi_{\text{c:v}}$. This dimensional result is valid for $\overline{h}_{\text{channels}} = 1132$ W/m·K (overall heat transfer coefficient of non-membrane regions) and $\dot{m}_{\text{f,in}}/w = 0.0833$ kg/m-s.

The maximum length and NTU are strong functions of $\phi_{\text{ch:m}}$ and ΔT_{VPD} and are affected less by $\phi_{\text{c:v}}$. Note that the value of GOR^{crit} is significantly affected by $\phi_{\text{c:v}}$ (as shown in Appendix A.8), evidenced by the difference in performance between AGMD and CGMD (with a thick membrane). The maximum module length is extremely high at low salinities as long as $\phi_{\text{ch:m}}$ is small enough (i.e., if the membrane is thick and heat transfer coefficients of non-membrane elements are high). At larger feed salinity, the maximum allowable length decreases (even for a relatively thick membrane). Similarly, as $\phi_{\text{ch:m}}$ increases (thinner membrane or higher resistances in parts of the module other than the membrane), the allowable maximum length decreases.

The GOR obtained by setting $L = L^{\max}$ is within 1% of the maximum GOR obtained by numerical optimization of the full 1-D module over a range of $s_{\text{in}} \in [70, 250]$ g/kg, $\phi_{\text{ch:m}} \in [0.05\text{–}1.15]$, and $\phi_{\text{c:v}} \in [3.1, 6.2]$.

3.3.3. Adjusting feed flow rate to avoid counter-productive operation

Winter et al. [36] noted the existence of a practically relevant value of NTU^{crit} or $\dot{m}_{\text{f}}^{\text{crit}}$ at high salinity based on experiments with large-scale PGMD modules (Fig. 16). Note that the experimental data at $s_{\text{f,in}} =$ 50 g/kg and 75 g/kg reach a maximum with changes in feed flow rate. The numerical model (now including the effect of feed flow on channel heat transfer coefficient) can also predict the existence of a critical flow rate and maximum GOR. If the flow rate is set based on the HX analogy model equation for NTU^{crit}, the

GOR obtained is very close to the numerical model's maximum GOR.

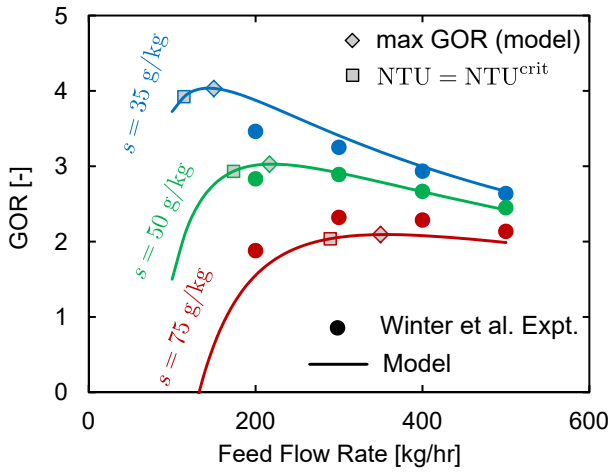

Figure 16: Effect of flowrate on maximum GOR (attained at $\mathrm{NTU}^{\mathrm{crit}}$) of a fixed size system at various salinity levels. Data from Winter et al. for PGMD [36]

4. Concluding remarks

The energy efficiency (GOR) and flux performance of common single stage MD configurations up to high feed salinity levels were compared in this study. The thermal resistance of the gap region in permeate/conductive gap MD directly corresponds to the resistance of the external HX in DCMD; both limit the extent of preheating of the feed stream. A low value of these thermal resistances results in improved GOR and flux irrespective of the salinity level. Simple permeate gap MD can be modified to the better CGMD by making the gap thinner or introducing a more conductive spacer material. To match CGMD's performance with DCMD, the external HX area has to be several times larger than the membrane, so as to match these resistances ($U_{\mathrm{HX}} A_{\mathrm{HX}} = h_{\mathrm{gap}} A_{\mathrm{MD}}$). The cost of increasing the gap conductance is likely to be lower than using a much larger HX, and hence overall, CGMD is preferred among these design variants.

AGMD is more resistant to higher feed salinity levels and achieves a higher GOR than the other configurations in large area modules. AGMD is brought within a common analytical framework together with the other systems by identifying the membrane along with the air-gap region together as an effectively thicker membrane. Care should be taken in AGMD systems to avoid partial or complete flooding of the air-gap which can push AGMD performance down towards that of PGMD. CGMD and DCMD with a thick membrane are also resistant to high salinity without being vulnerable to the negative effects of gap flooding during operation. An AGMD system without gap flooding outperforms CGMD with a thick membrane since the permeability coefficient of the open air-gap is higher and the thermal conductivity of the air gap is likely to be lower than that of the membrane.

The choice of optimal MD configuration has been linked here with the choice of optimal membrane thickness. This work presents a method to simultaneously pick a cost-optimal membrane thickness and

system size. GOR-flux operating curves can be plotted for several δ_{m} values and an upper-limit profile of these curves represents the best case design when allowing for variations in membrane thickness and system size. An operating point along this max-GOR flux operating curve, and its corresponding membrane thickness and membrane area, can be identified to minimize the specific cost of pure water production as a function of the ratio of specific cost of thermal energy to amortized system area.

At small size and low salinity, an increase in MD system specific area ($A/\dot{m}_{\mathrm{f}}$) results in an improvement in GOR and a decline in flux. However, beyond a critical system size, GOR also starts to decline rather than improve. As a result, irrespective of the costs of thermal energy and system area, there exists no justification to operating beyond this critical system size. This critical specific area can also be expressed non-dimensionally by $\mathrm{NTU}^{\mathrm{crit}}$. An analytical expression for $\mathrm{NTU}^{\mathrm{crit}}$ is derived using the simplified HX analogy model of MD, as a function of feed salinity (ΔT_{VPD}) and the two non-dimensional resistance ratios, $\phi_{\mathrm{c:v}}$ and $\phi_{\mathrm{ch:m}}$. This expression can inform the choice of system size at the design stage (for treating a given feed flow rate) or the selection of flow rate during operation (for a physical system of fixed size) so as to avoid the counterproductive operating regime.

Acknowledgments

JS thanks the Tata Center for Technology and Design at MIT for funding this work. HWC thanks Kuwait Foundation for the Advancement Sciences (KFAS) for their financial support through Project No. P31475EC01.

The authors would like to acknowledge Bailey Montano, Luke Roberto, and Elizabeth Vasquez for assisting with experiments.

Appendix A. Appendix

Appendix A.1. Economic analysis

The flux-GOR performance curve for a given MD configuration indicates the set of all operating points that are accessible to the technology by varying system size at fixed feed flow rate. The overall specific cost of water production from an MD system is influenced by both capital and operating expenditures. The capital cost increases with system size. The operating expense consists of labor, chemicals, membrane and other material replacement, as well as energy. Energy is utilized in an MD system both in the form of heat and electricity. Considering only the cost of capital (assuming capital cost is linearly proportional to membrane area) and energy consumption, the overall cost of water from MD can be written as a function of three terms:

$$c = c_{\mathrm{CapEx}} + c_{\mathrm{thermal}} + c_{\mathrm{electric}} \tag{A.1}$$

c_{CapEx} can be expressed as a function of water flux as:

$$\begin{aligned} c_{\mathrm{CapEx}}[\$/\mathrm{m}^3] &= \frac{C_{\mathrm{system,ammortized}}[\$/\mathrm{hr}]}{\dot{\mathrm{V}}_{\mathrm{p}}[\mathrm{m}^3/\mathrm{hr}]} = \frac{c_{\mathrm{sp,capital}}[\$/\mathrm{m}^2] \times A[\mathrm{m}^2] \times \mathrm{CAF}[\mathrm{hr}^{-1}]}{J[\mathrm{Lm}^{-2}\mathrm{hr}^{-1}] \times A[\mathrm{m}^2] \times 10^{-3}[\mathrm{m}^3/\mathrm{L}]} \\ &= \frac{C_{\mathrm{flux}}}{J} \end{aligned} \tag{A.2}$$

For a 20 year plant life and annual interest rate of 10%, the capital amortization factor CAF = $1.35 \times 10^{-5}[\mathrm{hr}^{-1}]$. For a system specific cost of c_{sp} =\$100/m^2, $C_{\mathrm{flux}} = 1.35$ [\$-L/m^5·hr] and $c_{\mathrm{CapEx}} = \frac{1.35}{J}$.

The contribution of thermal energy cost to the cost of water produced by MD is directly proportional to the specific cost of thermal energy and the specific thermal energy consumption of the MD process.

$$\begin{aligned} c_{\mathrm{thermal}}[\$/\mathrm{m}^3] &= c_{sp,thermal}[\$/\mathrm{kWh}] \times q_{\mathrm{MD}}[\mathrm{kWh/m}^3] \\ &= c_{sp,thermal}[\$/\mathrm{MMBTU}] \times \frac{h_{\mathrm{fg}}[\mathrm{J/kg}]}{\mathrm{GOR}} \times (0.947 \times 10^{-9})[\mathrm{MMBTU/J}] \times 10^3[\mathrm{kg/m}^3] \\ &= \frac{C_{\mathrm{GOR}}}{\mathrm{GOR}} \end{aligned} \tag{A.3}$$

Considering the cost of energy from natural gas to be \$13.11/MMBTU (2005 data [62]) and $h_{\mathrm{fg}} = 2.442 \times 10^6$ J/kg, $C_{\mathrm{GOR}} = 30.34[\$/\mathrm{m}^3]$ and $c_{\mathrm{thermal}} = \frac{30.34}{\mathrm{GOR}}$. Based on the current price of natural gas, or with the use of other waste heat sources, the cost of thermal energy would be lower and hence results are plotted for a range of $C_{\mathrm{GOR}}/C_{\mathrm{flux}} = 22.6$–1.

If $\dot{W}$ is the electricity consumption in watts, the corresponding contribution to the overall specific cost of water can be written as

$$\begin{aligned} c_{\mathrm{electric}} &= c_{\mathrm{sp,electric}}[\$/\mathrm{kWh}] \times w_{sp,electric}[\mathrm{kWh/m}^3] \\ &= c_{\mathrm{sp,electric}}[\$/\mathrm{kWh}] \times \frac{\dot{W}[\mathrm{W}] \times \cancel{10^{-3}}[\mathrm{kW/W}] \times \cancel{1}\,\mathrm{hr}}{J[\mathrm{Lm}^{-2}\mathrm{hr}^{-1}] \times A[\mathrm{m}^2] \times \cancel{10^{-3}}[\mathrm{m}^3/\cancel{L}] \times \cancel{1}\,\mathrm{hr}} \\ &= \frac{c_{\mathrm{sp,electric}}\left(\frac{\dot{W}}{A}\right)}{J} \\ &= \frac{C'_{\mathrm{pump}}}{J} \end{aligned} \tag{A.4}$$

Unlike C_{flux} and C_{GOR}, C'_{pump} is not independent of system size, as the pumping power increases with an increase in module length. Duong et al. report a low value of around 0.3 kWh/m^3 for the specific electrical energy consumption [63]. Nevertheless, even for a pump power consumption of 1–2 kWh/m^3-product, the relative contribution of pump energy consumption is much lower than that of capital cost and thermal energy. As a result, the total cost of water from MD can be approximated as

$$c \approx c_{\mathrm{CapEx}} + c_{\mathrm{thermal}} = \frac{C_{\mathrm{flux}}}{J} + \frac{C_{\mathrm{GOR}}}{\mathrm{GOR}} \tag{A.5}$$

Appendix A.2. Baseline system parameters

See Table A.2.

Table A.2: Baseline system parameters.

Parameter	Symbol	Value	Units
Membrane permeability coefficient	B_0	1.5×10^{-10}	s
Membrane thickness	δ_{m}	200	μm
Membrane porosity	ϕ	0.8	-
Membrane material conductivity	k_{m}	0.2	W/m-K
Membrane width per unit flow rate	$w/\dot{m}_{\mathrm{f,in}}$	12	m/(kg/s)
Top temperature	$T_{\mathrm{f,in}}$	85	°C
Bottom temperature	$T_{\mathrm{c,in}}$	25	°C
Channel height	d_{ch}	1	mm
Gap thickness	d_{gap}	1	mm
CGMD - gap conductivity	k_{gap}	10	W/m-K
PGMD - gap conductivity	k_{gap}	0.6	W/m-K
AGMD - gap porosity	ϕ_{gap}	0.9	-
AGMD - gap spacer conductivity	$k_{\mathrm{gap,spacer}}$	0.2	W/m-K
DCMD - HX Area ratio	$A_{\mathrm{HX}}/A_{\mathrm{m}}$	1	-
DCMD - HX heat transfer coefficient	U_{HX}	1300	W/m^2-K

Appendix A.3. Balanced MD systems

Figure A.17 shows the flow profiles for balanced DCMD [40] and gap MD systems [41], along with the temperature variation within balanced HXs.

Appendix A.4. Two balanced HXs with an intermediate fluid

For the system shown in Fig. 3, since the HX are balanced, the temperature drop of one stream is equal to the temperature gain of the other:

$$\Delta T_{\mathrm{ax}} = T_{\mathrm{h,in}} - T_{\mathrm{h,out}} = T_{\mathrm{i},1} - T_{\mathrm{i},2} = T_{\mathrm{c,out}} - T_{\mathrm{c,in}}$$

For the individual HXs:

$$\varepsilon_{\mathrm{a}} = \frac{T_{\mathrm{i},1} - T_{\mathrm{i},2}}{T_{\mathrm{h,in}} - T_{\mathrm{i},2}} = \frac{\mathrm{NTU_a}}{1 + \mathrm{NTU_a}} \tag{A.6}$$

$$\varepsilon_{\mathrm{b}} = \frac{T_{\mathrm{c,out}} - T_{\mathrm{c,in}}}{T_{\mathrm{i},1} - T_{\mathrm{c,in}}} = \frac{\mathrm{NTU_b}}{1 + \mathrm{NTU_b}} \tag{A.7}$$

Rearranging,

$$\frac{1}{\varepsilon_{\mathrm{a}}} = \frac{T_{\mathrm{h,in}} - T_{\mathrm{i},2}}{\Delta T_{\mathrm{ax}}} = 1 + \frac{1}{\mathrm{NTU_a}} \tag{A.8}$$

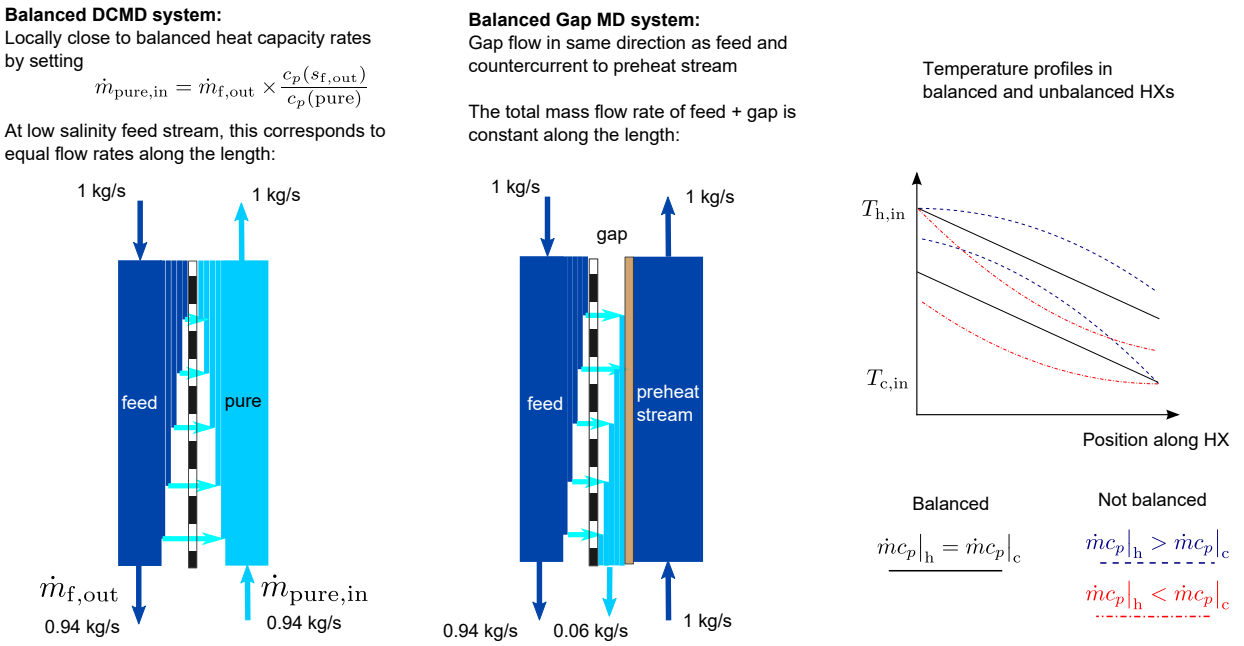

Figure A.17: Flows in balanced MD systems.

$$\frac{1}{\varepsilon_{\mathrm{b}}} = \frac{T_{\mathrm{i},1} - T_{\mathrm{c,in}}}{\Delta T_{\mathrm{ax}}} = 1 + \frac{1}{\mathrm{NTU}_{\mathrm{b}}} \tag{A.9}$$

Similarly, for the overall HX (without any subscript):

$$\frac{1}{\varepsilon} = \frac{T_{\mathrm{h,in}} - T_{\mathrm{c,in}}}{\Delta T_{\mathrm{ax}}} = 1 + \frac{1}{\mathrm{NTU}} \tag{A.10}$$

$$\begin{aligned}
\frac{1}{\varepsilon} &= \frac{1}{\Delta T_{\mathrm{ax}}} \times (T_{\mathrm{h,in}} - T_{\mathrm{i},2} + T_{\mathrm{i},1} - T_{\mathrm{c,in}} - (T_{\mathrm{i},1} - T_{\mathrm{i},2})) \\
&= \frac{1}{\Delta T_{\mathrm{ax}}} \times ((T_{\mathrm{h,in}} - T_{\mathrm{i},2}) + (T_{\mathrm{i},1} - T_{\mathrm{c,in}}) - \Delta T_{\mathrm{ax}}) \\
&= \frac{1}{\varepsilon_{\mathrm{a}}} + \frac{1}{\varepsilon_{\mathrm{b}}} - 1 \\
&= \left(1 + \frac{1}{\mathrm{NTU}_{\mathrm{a}}}\right) + \left(1 + \frac{1}{\mathrm{NTU}_{\mathrm{b}}}\right) - 1 \\
&= 1 + \left(\frac{1}{\mathrm{NTU}_{\mathrm{a}}} + \frac{1}{\mathrm{NTU}_{\mathrm{b}}}\right)
\end{aligned} \tag{A.11}$$

From Eqs. A.10, A.11:

$$\begin{aligned}
\frac{1}{\mathrm{NTU}} &= \frac{1}{\mathrm{NTU}_{\mathrm{a}}} + \frac{1}{\mathrm{NTU}_{\mathrm{b}}} \\
\rightarrow \frac{1}{(UA)} &= \frac{1}{(UA)_{\mathrm{a}}} + \frac{1}{(UA)_{\mathrm{b}}}
\end{aligned} \tag{A.12}$$

Appendix A.5. Potential for flooding in AGMD

The present numerical model is compared against results from the pilot scale MD module reported in [63]. The GOR-flux values obtained with changes in feed flow rate (Fig. A.18a) and top temperature (Fig. A.18b)

at two values of salinity $s_{\text{in}} = 0, 35$ g/kg are plotted. The channel geometry, feed flow rate, temperature and salinity in the numerical model are set based on the reported data.

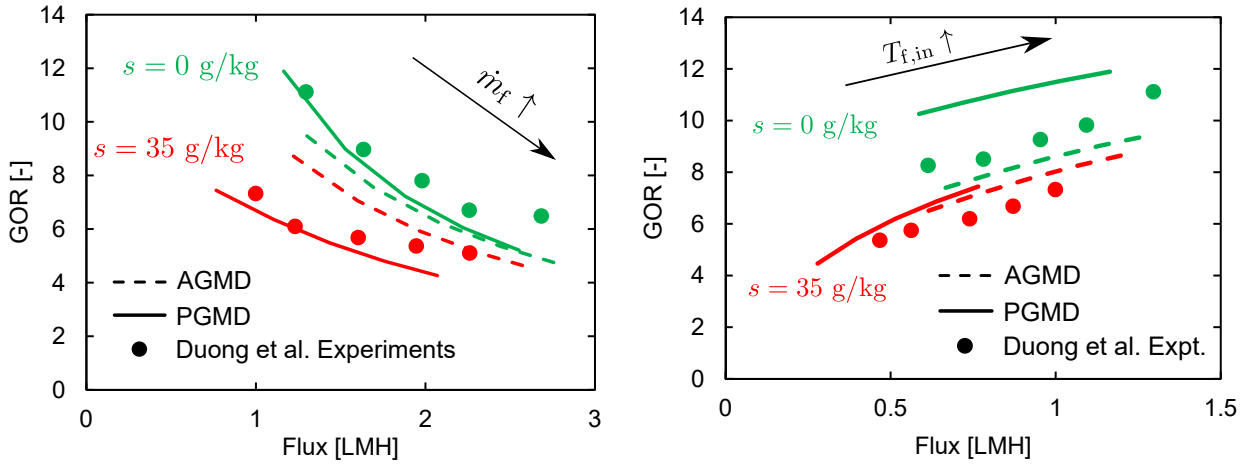

(a) Validation at various feed flow rates.

(b) Validation at various feed inlet temperatures

Figure A.18: Comparison of the full-system model by comparing against published data for flux and energy efficiency. AG (dotted model lines) refers to Air Gap and PG to Permeate Gap (solid model lines). The reported module geometry data was input to the model. Additionally the following parameters were used: $B_0 = 1.5 \times 10^{-10}$ kg/m·s·Pa, $h_{\text{ch}} \approx 5000$ W/m^2·K, $h_{\text{gap}}^{\text{PGMD}} = 500$ W/m^2·K, $d_{\text{gap,eff}}^{\text{AGMD}} = 0.7$ mm.

The decline in performance between $s_{\text{in}} = 0$ and 35 g/kg cases is more pronounced then what would be expected for an ideal air gap system. The AGMD model prediction shows a small difference in performance between the two salinity levels, whereas the difference predicted by the PGMD model is closer to the observed trend. We can therefore surmise that the large scale experimental module could have had some water bridging or partial flooding of the gap. On average, experimental results occur between the model predictions for an air-gap system and that of a permeate gap system (where the entire gap is assumed to be filled with produced product water).

Note that in Fig. A.18a, at larger feed flow rates, the obtained GOR and flux values are higher than predicted by both the AGMD and PGMD models. This could be because a simple laminar correlation is used for the heat transfer coefficient within the flow channels in the model, whereas in reality, with an increase in flow rate, the effective heat transfer coefficient would increase due to increased mixing in the spacer-filled channel. Additionally, the effect of changes in top temperature on B_0 of the membrane have also not been considered in the numerical model.

Appendix A.6. Effect of salt on vapor pressure depression

The presence of solutes leads to a reduction in the vapor pressure of the feed solution. At very low solute concentrations, this effect can be evaluated through Raoult's law. For non-ideal solutions,

$$p^{\text{vap}}(T, s) = P_{\text{sat}}(T) a_{\text{w}}(T, s) \tag{A.13}$$

where a_w is the activity of water.

In order to include the vapor transport resistance into the HX analogy model, the vapor pressure of pure water was approximated as an exponential function of temperature. Correspondingly, the effect of salt on reducing the vapor pressure was incorporated as an effective reduction in the temperature of the feed solution which results in a lower vapor pressure. A vapor pressure depression temperature (ΔT_{VPD}) can be defined as a function of temperature and salinity such that,

$$p^{\mathrm{vap}}(T,s) = p^{\mathrm{vap}}(T - \Delta T_{\mathrm{VPD}}(T,s), s=0) = P_{\mathrm{sat}}(T - \Delta T_{\mathrm{VPD}}(T,s)) \tag{A.14}$$

A more commonly used ΔT metric is the boiling point elevation or ΔT_{BPE} which is defined such that:

$$p^{\mathrm{vap}}(T + \Delta T_{\mathrm{BPE}}(T,s), s) = p^{\mathrm{vap}}(T, s=0) = P_{\mathrm{sat}}(T) \tag{A.15}$$

or in other words, the additional temperature required for a salty solution to match the vapor pressure of a pure water solution.

Both ΔT_{VPD} and ΔT_{BPE} are represented pictorially in Fig. A.19. $p^{\mathrm{vap}}(T,s)$ for sodium chloride solution is obtained from Pitzer's model [49]. Over the range of temperatures and feed salinities relevant to MD, $\Delta T_{\mathrm{VPD}} \approx \Delta T_{\mathrm{BPE}}$ with a maximum deviation of about 3%, occurring at high salinity and temperature. This difference is lower than the uncertainty caused by the average feed salinity within the MD module, $T_{\mathrm{p,avg}}$. In this study, the following approximation was used: $p^{\mathrm{vap}}(T,s) \approx P_{\mathrm{sat}}\,(T - \Delta T_{\mathrm{BPE}})$.

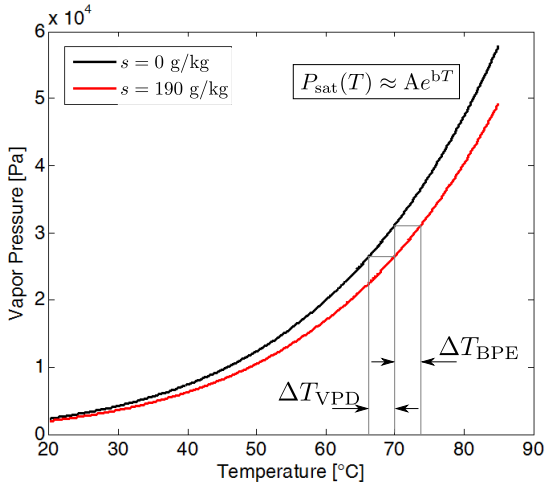

Figure A.19: Difference between ΔT_{VPD} and ΔT_{BRE} illustrated for a solution at $T = 70\,^{\circ}\mathrm{C}$ and $s = 190$ g/kg.

Appendix A.7. Effect of non-dimensional parameters on flux

While GOR is only a function of the non-dimensional parameters $\phi_{\mathrm{ch:m}}$, $\phi_{\mathrm{c:v}}$ and system size (NTU), flux is additionally a function of the magnitudes of the resistances (related to design goal 1, of maximizing overall heat transfer coefficient, U). Hence GOR-flux performance curves obtained by allowing system size to change, at the same set of resistance ratios, can be different based on the resistance magnitudes.

Figure A.20a shows the effect of decreasing $\phi_{\text{ch:m}}$ in two ways: keeping membrane thickness constant while increasing h_{ch} and maintaining a constant h_{ch} while increasing δ_{m}. While the maximum GOR value is the same for these two cases, flux for the case with higher channel transfer coefficient is about two times higher than the case with a thicker membrane.

When $\phi_{\text{ch:m}}$ is reduced to 0.2 from 0.4 by increasing membrane thickness, GOR is higher at low flux, but beyond 4 LMH, the original system $\phi_{\text{ch:m}} = 0.4$ outperforms the modified system, in spite of $\phi_{\text{ch:m}}$ being lower (compare the red and black curves). On the other hand, when $\phi_{\text{ch:m}}$ is reduced by increasing h_{ch}, the green curve outperforms the black curve over all flux levels.

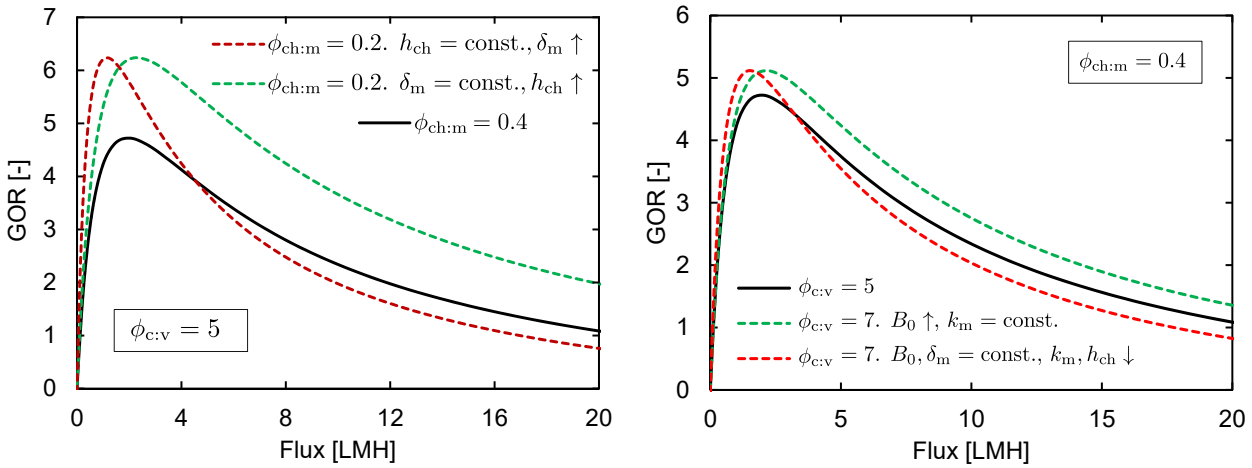

(a) The effect of actual transfer coefficient on flux at the same value of $\phi_{\text{ch:m}}$.

(b) The effect of actual transfer coefficient on flux at the same value of $\phi_{\text{c:v}}$.

Figure A.20: Max GOR is only a function of $\phi_{\text{c:v}}$ and $\phi_{\text{ch:m}}$, but flux depends on the magnitudes of the resistances also. $s_{\text{in}=150}$ g/kg.

Similarly, Fig. A.20b shows the difference in performance based on whether $\phi_{\text{c:v}}$ is increased by improving membrane mass transfer or by increasing membrane heat transfer resistance, while keeping $\phi_{\text{ch:m}}$ and δ_{m} constant in both cases. In order to maintain a constant $\phi_{\text{ch:m}}$ and δ_{m}, a decrease in k_{m} would also be accompanied by lower h_{ch}. It is better to increase $\phi_{\text{c:v}}$ by increasing B_0 rather than by decreasing k_{m}, at fixed $\phi_{\text{ch:m}}$.

Appendix A.8. Importance of $\phi_{\text{c:v}}$ for maximum GOR

While it was observed that $\phi_{\text{c:v}}$ or good membrane design has a small effect on NTU^{crit}, its effect on the actual magnitude of the maximum GOR achieved at the critical size is more significant, as illustrated in Fig. A.21.

The way to read this chart is as follows: For a feed salinity of 200 g/kg and $\phi_{\text{ch:m}} = 0.2$, the maximum GOR achievable (at the critical system size) is 5 for $\phi_{\text{c:v}} = 10$. If, on the other hand, $\phi_{\text{c:v}} = 2.5$, the

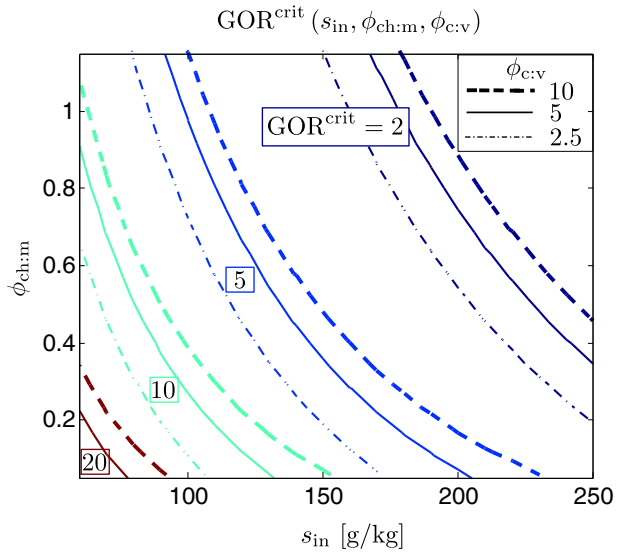

Figure A.21: Effect of vapor permeability to heat conductivity ratio ($\phi_{\mathrm{c:v}}$) on maximum GOR of the system.

maximum GOR (interpolated from the chart) is only about 3. The impact of $\phi_{\mathrm{c:v}}$ on GOR is significant, even though it has a small effect on $\mathrm{NTU}^{\mathrm{crit}}$.

References

[1] C. Fritzmann, J. Löwenberg, T. Wintgens, T. Melin, State-of-the-art of reverse osmosis desalination, Desalination 216 (1–3) (2007) 1–76. doi:10.1016/j.desal.2006.12.009.
URL http://www.sciencedirect.com/science/article/pii/S0011916407004250

[2] G. P. Thiel, E. W. Tow, L. D. Banchik, H. W. Chung, J. H. Lienhard V, Energy consumption in desalinating produced water from shale oil and gas extraction, Desalination 366 (2015) 94–112. doi:http://dx.doi.org/10.1016/j.desal.2014.12.038.
URL http://www.sciencedirect.com/science/article/pii/S0011916414006857

[3] B. Ericsson, B. Hallmans, Treatment of saline wastewater for zero discharge at the debiensko coal mines in poland, Desalination 105 (1) (1996) 115 – 123. doi:http://dx.doi.org/10.1016/0011-9164(96)00065-3.
URL http://www.sciencedirect.com/science/article/pii/0011916496000653

[4] L. M. Vane, Water recovery from brines and salt-saturated solutions: operability and thermodynamic efficiency considerations for desalination technologies, Journal of Chemical Technology & Biotechnologydoi:10.1002/jctb.5225.
URL http://dx.doi.org/10.1002/jctb.5225

[5] R. K. McGovern, G. P. Thiel, G. P. Narayan, S. M. Zubair, J. H. Lienhard V, Performance limits of zero and single extraction humidification-dehumidification desalination systems, Applied Energy 102 (2013) 1081 – 1090. doi:http://dx.doi.org/10.1016/j.apenergy.2012.06.025.
URL http://www.sciencedirect.com/science/article/pii/S0306261912004709

[6] G. P. Narayan, M. G. S. John, S. M. Zubair, J. H. Lienhard V, Thermal design of the humidification dehumidification desalination system: An experimental investigation, International Journal of Heat and Mass Transfer 58 (1) (2013) 740–748. doi:http://doi.org/10.1016/j.ijheatmasstransfer.2012.11.035.
URL http://www.sciencedirect.com/science/article/pii/S0017931012008903

[7] K. M. Chehayeb, G. P. Narayan, S. M. Zubair, J. H. Lienhard V, Use of multiple extractions and injections to thermodynamically balance the humidification dehumidification desalination system, International Journal of Heat and Mass Transfer 68 (2014) 422 – 434.
URL http://www.sciencedirect.com/science/article/pii/S0017931013007990

[8] K. M. Chehayeb, G. P. Narayan, S. M. Zubair, J. H. Lienhard V, Thermodynamic balancing of a fixed-size two-stage humidification dehumidification desalination system, Desalination 369 (2015) 125–139. doi:10.1016/j.desal.2015.04.021.
URL http://www.sciencedirect.com/science/article/pii/S0011916415002660

[9] T. Pankratz, HDH tackles brine disposal challenge, Water Desalination Report 50 (17) (2014) 2–3.

[10] K. M. Chehayeb, J. H. Lienhard V, Effect of feed salinity on the performance of humidification dehumidification desalination, in: The International Desalination Association World Congress on Desalination and Water Reuse, San Diego, USA, 2015.
URL http://web.mit.edu/lienhard/www/papers/conf/CHEHAYEB_IDA_San_Diego_2015.pdf

[11] L. M. Camacho, L. Dumée, J. Zhang, J.-d. Li, M. Duke, J. Gomez, S. Gray, et al., Advances in membrane distillation for water desalination and purification applications, Water 5 (1) (2013) 94–196. doi:10.3390/w5010094.
URL http://www.mdpi.com/2073-4441/5/1/94/

[12] E. Drioli, A. Ali, F. Macedonio, Membrane distillation : Recent developments and perspectives, Desalination 356 (2015) 56–84. doi:10.1016/j.desal.2014.10.028.
URL http://dx.doi.org/10.1016/j.desal.2014.10.028

[13] C. R. Martinetti, A. E. Childress, T. Y. Cath, High recovery of concentrated RO brines using forward osmosis and membrane distillation, Journal of Membrane Science 331 (1–2) (2009) 31 – 39. doi:10.1016/j.memsci.2009.01.003.
URL http://www.sciencedirect.com/science/article/pii/S037673880900012X

[14] P. Xu, T. Y. Cath, A. P. Robertson, M. Reinhard, L. J. O., J. E. Drewes, Critical review of desalination concentrate management, treatment and beneficial use, Environmental Engineering Science 30 (2013) 502–514. doi:10.1089/ees.2012.0348.
URL https://doi.org/10.1089/ees.2012.0348

[15] T. Tong, M. Elimelech, The global rise of zero liquid discharge for wastewater management: Drivers, technologies, and future directions, Environmental Science & Technology 50 (13) (2016) 6846–6855. doi:10.1021/acs.est.6b01000.
URL http://dx.doi.org/10.1021/acs.est.6b01000

[16] R. Sarbatly, C.-K. Chiam, Evaluation of geothermal energy in desalination by vacuum membrane distillation, Applied Energy 112 (2013) 737–746. doi:10.1016/j.apenergy.2012.12.028.
URL http://www.sciencedirect.com/science/article/pii/S0306261912009105

[17] N. Ghaffour, S. Lattemann, T. Missimer, K. C. Ng, S. Sinha, G. Amy, Renewable energy-driven innovative energy-efficient desalination technologies, Applied Energy 136 (2014) 1155–1165. doi:10.1016/j.apenergy.2014.03.033.
URL http://www.sciencedirect.com/science/article/pii/S0306261914002633

[18] G. Zaragoza, A. Ruiz-Aguirre, E. Guillén-Burrieza, Efficiency in the use of solar thermal energy of small membrane desalination systems for decentralized water production, Applied Energy 130 (2014) 491–499.

doi:10.1016/j.apenergy.2014.02.024.
URL http://www.sciencedirect.com/science/article/pii/S0306261914001603

[19] M. Baghbanzadeh, D. Rana, C. Q. Lan, T. Matsuura, Zero thermal input membrane distillation, a zero-waste and sustainable solution for freshwater shortage, Applied Energy 187 (2017) 910 – 928. doi:http://dx.doi.org/10.1016/j.apenergy.2016.10.142.
URL http://www.sciencedirect.com/science/article/pii/S0306261916314799

[20] S. Adham, A. Hussain, J. M. Matar, R. Dores, A. Janson, Application of membrane distillation for desalting brines from thermal desalination plants, Desalination 314 (2013) 101 – 108. doi:10.1016/j.desal.2013.01.003.
URL http://www.sciencedirect.com/science/article/pii/S0011916413000088

[21] Y. Yun, R. Ma, W. Zhang, A. Fane, J. Li, Direct contact membrane distillation mechanism for high concentration NaCl solutions, Desalination 188 (2006) 251–262.
URL http://www.sciencedirect.com/science/article/pii/S0011916406000567

[22] M. Safavi, T. Mohammadi, High-salinity water desalination using VMD, Chemical Engineering Journal 149 (1–3) (2009) 191 – 195. doi:10.1016/j.cej.2008.10.021.
URL http://www.sciencedirect.com/science/article/pii/S1385894708006980

[23] Y. Guan, J. Li, F. Cheng, J. Zhao, X. Wang, Influence of salt concentration on DCMD performance for treatment of highly concentrated NaCl, KCl, $MgCl_2$ and $MgSO_4$ solutions, Desalination 355 (2015) 110–117. doi:10.1016/j.desal.2014.10.005.
URL http://linkinghub.elsevier.com/retrieve/pii/S0011916414005281

[24] B. Li, K. K. Sirkar, Novel membrane and device for vacuum membrane distillation-based desalination process, Journal of Membrane Science 257 (2005) 60–75. doi:10.1016/j.memsci.2004.08.040.
URL http://www.sciencedirect.com/science/article/pii/S0376738804008452

[25] A. Alkhudhiri, N. Darwish, N. Hilal, Treatment of high salinity solutions: Application of air gap membrane distillation, Desalination 287 (2012) 55 – 60. doi:10.1016/j.desal.2011.08.056.
URL http://www.sciencedirect.com/science/article/pii/S0011916411007715

[26] S. Al-Obaidani, E. Curcio, F. Macedonio, G. D. Profio, H. Al-Hinai, E. Drioli, Potential of membrane distillation in seawater desalination: Thermal efficiency, sensitivity study and cost estimation, Journal of Membrane Science 323 (1) (2008) 85 – 98. doi:dx.doi.org/10.1016/j.memsci.2008.06.006.
URL http://www.sciencedirect.com/science/article/pii/S0376738808005577

[27] L. Eykens, I. Hitsov, K. De Sitter, C. Dotremont, L. Pinoy, I. Nopens, B. Van der Bruggen, Influence Of Membrane Thickness And Process Conditions On Direct Contact Membrane Distillation At Different

Salinities, Journal of Membrane Science 498 (2015) 353–364. doi:10.1016/j.memsci.2015.07.037.
URL http://linkinghub.elsevier.com/retrieve/pii/S0376738815300661

[28] A. E. C. Francisco Suárez, Scott W. Tyler, A theoretical study of a direct contact membrane distillation system coupled to a salt-gradient solar pond for terminal lakes reclamation, Water Research 44 (12) (2010) 4601–4615. doi:10.1016/j.watres.2010.05.050.
URL http://www.sciencedirect.com/science/article/pii/S0043135410003672

[29] M. Khayet, T. Matsuura, Membrane Distillation Principles and Applications, Elsevier, 2011.

[30] F. Edwie, T.-S. Chung, Development of simultaneous membrane distillationcrystallization (smdc) technology for treatment of saturated brine, Chemical Engineering Science 98 (2013) 160 – 172. doi:http://dx.doi.org/10.1016/j.ces.2013.05.008.
URL http://www.sciencedirect.com/science/article/pii/S0009250913003291

[31] C. A. Quist-Jensen, A. Ali, S. Mondal, F. Macedonio, E. Drioli, A study of membrane distillation and crystallization for lithium recovery from high-concentrated aqueous solutions, Journal of Membrane Science 505 (2016) 167 – 173. doi:http://dx.doi.org/10.1016/j.memsci.2016.01.033.
URL http://www.sciencedirect.com/science/article/pii/S0376738816300333

[32] J. Swaminathan, H. W. Chung, D. M. Warsinger, J. H. Lienhard V, Membrane distillation model based on heat exchanger theory and configuration comparison, Applied Energy 184 (2016) 491 – 505. doi:10.1016/j.apenergy.2016.09.090.
URL http://www.sciencedirect.com/science/article/pii/S0306261916313927

[33] H. W. Chung, J. Swaminathan, D. M. Warsinger, J. H. Lienhard V, Multistage vacuum membrane distillation (MSVMD) systems for high salinity applications, Journal of Membrane Science 497 (2016) 128–141. doi:10.1016/j.memsci.2015.09.009.
URL http://www.sciencedirect.com/science/article/pii/S0376738815301733

[34] A. Deshmukh, M. Elimelech, Understanding the impact of membrane properties and transport phenomena on the energetic performance of membrane distillation desalination, Journal of Membrane Science 539 (2017) 458 – 474. doi:http://dx.doi.org/10.1016/j.memsci.2017.05.017.
URL http://www.sciencedirect.com/science/article/pii/S0376738817308323

[35] L. Martínez, J. M. Rodríguez-Maroto, On transport resistances in direct contact membrane distillation, Journal of Membrane Science 295 (1-2) (2007) 28–39. doi:10.1016/j.memsci.2007.02.029.
URL http://www.sciencedirect.com/science/article/pii/S0376738807001299

[36] D. Winter, J. Koschikowski, M. Wieghaus, Desalination using membrane distillation: Experimental studies on full scale spiral wound modules, Journal of Membrane Science 375 (1-2) (2011) 104–112.

doi:10.1016/j.memsci.2011.03.030.
URL http://linkinghub.elsevier.com/retrieve/pii/S0376738811002067

[37] A. Alklaibi, N. Lior, Comparative Study of Direct Contact and Air Gap Membrane Distillation Processes, Ind. Eng. Chem. Res 2 (46) (2007) 584–590. doi:10.1021/ie051094u.
URL http://pubs.acs.org/doi/abs/10.1021/ie051094u

[38] L. Eykens, T. Reyns, K. D. Sitter, C. Dotremont, L. Pinoy, B. V. der Bruggen, How to select a membrane distillation configuration? process conditions and membrane influence unraveled, Desalination 399 (2016) 105 – 115. doi:http://dx.doi.org/10.1016/j.desal.2016.08.019.
URL http://www.sciencedirect.com/science/article/pii/S0011916416302533

[39] D. Winter, Membrane distillation - a thermodynamic, technological and economic analysis, Ph.D. thesis, University of Kaiserslautern, Germany (2015).
URL http://www.reiner-lemoine-stiftung.de/pdf/dissertationen/Dissertation-Winter.pdf

[40] J. Swaminathan, H. W. Chung, D. M. Warsinger, J. H. Lienhard V, Simple method for balancing direct contact membrane distillation, Desalination 383 (2016) 53 – 59. doi:10.1016/j.desal.2016.01.014.
URL http://www.sciencedirect.com/science/article/pii/S0011916416300133

[41] J. Swaminathan, H. W. Chung, D. Warsinger, F. Al-Marzooqi, H. A. Arafat, J. H. Lienhard V, Energy efficiency of permeate gap and novel conductive gap membrane distillation, Journal of Membrane Science 502 (2016) 171–178. doi:10.1016/j.memsci.2015.12.017.
URL http://www.sciencedirect.com/science/article/pii/S0376738815303616

[42] M. I. Ali, E. K. Summers, H. A. Arafat, J. H. Lienhard V, Effects of membrane properties on water production cost in small scale membrane distillation systems, Desalination 306 (2012) 60 – 71. doi:http://dx.doi.org/10.1016/j.desal.2012.07.043.
URL http://www.sciencedirect.com/science/article/pii/S0011916412004262

[43] R. B. Saffarini, E. K. Summers, H. A. Arafat, J. H. Lienhard V, Economic evaluation of stand-alone solar powered membrane distillation systems, Desalination 299 (2012) 55–62. doi:10.1016/j.desal.2012.05.017.
URL http://www.sciencedirect.com/science/article/pii/S0011916412002779

[44] H. Y. Wu, R. Wang, R. W. Field, Direct contact membrane distillation: An experimental and analytical investigation of the effect of membrane thickness upon transmembrane flux, Journal of Membrane Science 470 (2014) 257 – 265. doi:http://dx.doi.org/10.1016/j.memsci.2014.06.002.
URL http://www.sciencedirect.com/science/article/pii/S0376738814004487

[45] L. Martinez, J. Rodriguez-Maroto, Membrane thickness reduction effects on direct contact membrane distillation performance, Journal of Membrane Science 312 (1-2) (2008) 143 – 156. doi:http://dx.

doi.org/10.1016/j.memsci.2007.12.048.
URL http://www.sciencedirect.com/science/article/pii/S0376738808000082

[46] A. Ali, C. Quist-Jensen, F. Macedonio, E. Drioli, On designing of membrane thickness and thermal conductivity for large scale membrane distillation modules, Journal of Membrane Science and Research 2 (4) (2016) 179–185. doi:10.22079/jmsr.2016.21948.
URL http://www.msrjournal.com/article_21948.html

[47] E. K. Summers, H. A. Arafat, J. H. Lienhard V, Energy efficiency comparison of single-stage membrane distillation (MD) desalination cycles in different configurations, Desalination 290 (2012) 54–66. doi:10.1016/j.desal.2012.01.004.
URL http://linkinghub.elsevier.com/retrieve/pii/S0011916412000264

[48] S.A.Klein, Engineering Equation Solver.
URL http://www.fchart.com/ees/

[49] K. S. Pitzer, J. C. Peiper, R. H. Busey, Thermodynamic Properties of Aqueous Sodium Chloride Solutions, Journal of Physical and Chemical Reference Data 13 (1) (1984) 1–102. doi:10.1063/1.555709.
URL http://scitation.aip.org/content/aip/journal/jpcrd/13/1/10.1063/1.555709

[50] D. M. Warsinger, E. W. Tow, J. Swaminathan, J. H. Lienhard V, Theoretical framework for predicting inorganic fouling in membrane distillation and experimental validation with calcium sulfate, Journal of Membrane Science 528 (2017) 381 – 390. doi:http://dx.doi.org/10.1016/j.memsci.2017.01.031.
URL http://www.sciencedirect.com/science/article/pii/S0376738817301916

[51] M. E. Leitch, C. Li, O. Ikkala, M. S. Mauter, G. V. Lowry, Bacterial nanocellulose aerogel membranes: Novel high-porosity materials for membrane distillation, Environmental Science & Technology Letters 3 (3) (2016) 85–91. arXiv:http://dx.doi.org/10.1021/acs.estlett.6b00030, doi:10.1021/acs.estlett.6b00030.
URL http://dx.doi.org/10.1021/acs.estlett.6b00030

[52] I. Hitsov, K. D. Sitter, C. Dotremont, P. Cauwenberg, I. Nopens, Full-scale validated air gap membrane distillation (agmd) model without calibration parameters, Journal of Membrane Science 533 (2017) 309 – 320. doi:http://doi.org/10.1016/j.memsci.2017.04.002.
URL http://www.sciencedirect.com/science/article/pii/S0376738816325170

[53] L. L. Morales, Visualization and measurement of filmwise and dropwise air gap membrane distillation at varied module inclination angle and gap spacer orientation, S.B. thesis, Massachusetts Institute of Technology (2016).
URL http://hdl.handle.net/1721.1/105688

[54] M. H. Sharqawy, L. D. Banchik, J. H. Lienhard V, Effectiveness–mass transfer units (ε–MTU) model of an ideal pressure retarded osmosis membrane mass exchanger, Journal of Membrane Science 445 (2013) 211–219. doi:10.1016/j.memsci.2013.06.027.
URL http://www.sciencedirect.com/science/article/pii/S0376738813005206

[55] L. D. Banchik, M. H. Sharqawy, J. H. Lienhard V, Effectiveness–mass transfer units (ε–MTU) model of a reverse osmosis membrane mass exchanger, Journal of Membrane Science 458 (2014) 189–198. doi:10.1016/j.memsci.2014.01.039.
URL http://www.sciencedirect.com/science/article/pii/S0376738814000520

[56] L. D. Banchik, M. H. Sharqawy, J. H. Lienhard V, Limits of power production due to finite membrane area in pressure retarded osmosis, Journal of Membrane Science 468 (2014) 81–89. doi:10.1016/j.memsci.2014.05.021.
URL http://www.sciencedirect.com/science/article/pii/S037673881400386X

[57] L. D. Banchik, , A. M. Weiner, B. Al Anzi, J. H. Lienhard V, System scale analytical modeling of forward and assisted forward osmosis mass exchangers with a case study on fertigation, Journal of Membrane Science 510 (2016) 533–545. doi:10.1016/j.memsci.2016.02.063.
URL http://www.sciencedirect.com/science/article/pii/S0376738816301211

[58] H. Y. Wu, M. Tay, R. W. Field, Novel method for the design and assessment of direct contact membrane distillation modules, Journal of Membrane Science 513 (2016) 260–269. doi:10.1016/j.memsci.2016.04.009.
URL http://www.sciencedirect.com/science/article/pii/S0376738816302204

[59] J. H. Lienhard V, J. H. Lienhard IV, A Heat Transfer Textbook, Fourth Edition, Dover Publications, Inc, 2011.
URL http://ahtt.mit.edu

[60] S. Bandini, C. Gostoli, G. Sarti, Role of heat and mass transfer in membrane distillation process, Desalination 81 (1) (1991) 91 – 106. doi:10.1016/0011-9164(91)85048-Y.
URL http://www.sciencedirect.com/science/article/pii/001191649185048Y

[61] E. K. Summers, J. H. Lienhard V, Experimental study of thermal performance in air gap membrane distillation systems including direct solar heating of membranes, Desalination 330 (2013) 100–111. doi:10.1016/j.desal.2013.09.023.
URL http://www.sciencedirect.com/science/article/pii/S0011916413004554

[62] U.S. Energy Information Administration, Henry hub natural gas spot price, https://www.eia.gov/dnav/ng/hist/rngwhhdm.htm (1997–2017).

[63] H. C. Duong, P. Cooper, B. Nelemans, T. Y. Cath, L. D. Nghiem, Evaluating energy consumption of air gap membrane distillation for seawater desalination at pilot scale level, Separation and Purification Technology 166 (2016) 55 – 62. doi:http://dx.doi.org/10.1016/j.seppur.2016.04.014.
URL http://www.sciencedirect.com/science/article/pii/S1383586616301897